MDPI

Article

Evaluation of SPI and Rainfall Departure Based on Multi-Satellite Precipitation Products for Meteorological Drought Monitoring in Tamil Nadu

Sellaperumal Pazhanivelan [1,*], **Vellingiri Geethalakshmi** [1], **Venkadesh Samykannu** [2], **Ramalingam Kumaraperumal** [3], **Mrunalini Kancheti** [4], **Ragunath Kaliaperumal** [1], **Marimuthu Raju** [1] and **Manoj Kumar Yadav** [5]

[1] Water Technology Centre, Tamil Nadu Agricultural University, Coimbatore 641003, India
[2] Agro-Climatic Research Centre, Tamil Nadu Agricultural University, Coimbatore 641003, India
[3] Department of Remote Sensing and GIS, Tamil Nadu Agricultural University, Coimbatore 641003, India
[4] Indian Council of Agricultural Research-Indian Institute of Pulses Research, Kanpur 208024, India
[5] Deutsche Gesellschaft für Internationale Zusammenarbeit (GIZ) GmbH, New Delhi 110029, India
[*] Correspondence: pazhanivelans@tnau.ac.in

Abstract: The prevalence of the frequent water stress conditions at present was found to be more frequent due to increased weather anomalies and climate change scenarios, among other reasons. Periodic drought assessment and subsequent management are essential in effectively utilizing and managing water resources. For effective drought monitoring/assessment, satellite-based precipitation products offer more reliable rainfall estimates with higher accuracy and spatial coverage than conventional rain gauge data. The present study on satellite-based drought monitoring and reliability evaluation was conducted using four high-resolution precipitation products, i.e., IMERGH, TRMM, CHIRPS, and PERSIANN, during the northeast monsoon season of 2015, 2016, and 2017 in the state of Tamil Nadu, India. These four precipitation products were evaluated for accuracy and confidence level by assessing the meteorological drought using standard precipitation index (SPI) and by comparing the results with automatic weather station (AWS) and rain gauge network data-derived SPI. Furthermore, considering the limited number of precipitation products available, the study also indirectly addressed the demanding need for high-resolution precipitation products with consistent temporal resolution. Among different products, IMERGH and TRMM rainfall estimates were found equipollent with the minimum range predictions, i.e., 149.8, 32.07, 80.05 mm and 144.31, 34.40, 75.01 mm, respectively, during NEM of 2015, 2016, and 2017. The rainfall data from CHIRPS were commensurable in the maximum range of 1564, 421, and 723 mm in these three consequent years (2015 to 2017) compared to AWS data. CHIRPS data recorded a higher per cent of agreement (>85%) compared to AWS data than other precipitation products in all the agro-climatic zones of Tamil Nadu. The SPI values were positive > 1.0 during 2015 and negative < −0.99 for 2016 and 2017, indicating normal/wet and dry conditions in the study area, respectively. This study highlighted discrepancies in the capability of the precipitation products IMERGH and TRMM estimates for low rainfall conditions and CHIRPS estimates in high rainfall regimes.

Keywords: drought; precipitation products; rainfall estimates; standard precipitation index

1. Introduction

Fluctuations in precipitation and other related climatic conditions can cause substantial damage to ecological habitats and agricultural production, degrading the economic and social stability of the region [1–3]. The high spatiotemporal variability and uncertainty of rainfall [4] significantly affect physical, biological, and human systems [5]. One of the most extreme climatic phenomena, drought, is known to have devastating effects on agriculture, water resources, and humid environments [6]. The increased prevalence of

drought-like conditions worldwide that could last for many years due to climate change and global warming increased the focus on drought studies in recent years. The incidence of the drought was predicted to grow in the following decades during 2020–2050 [7]. The repercussions of the drought on the social, economic, and political facets of our environment were profound [8]. Hence, appropriate pre-planning besides mitigation activities must be propagated and instigated to reduce the consequence of its effect [9].

The failure of the northeast monsoon in 2016 triggered one of the worst droughts in recorded history in the Tamil Nadu state of India, which declared all 32 districts drought-stricken [10]. In addition to posing a serious threat to agriculture and hydrology, the drought caused the state to suffer significant economic losses. In Tamil Nadu, it was observed that drought years became more frequent in recent decades. However, there are no comprehensive contingency measures to deal with or prepare for the drought. Though several studies addressed the issue at the district level, evaluating the aspects of drought and its interventions at agroclimatic zones or block levels would be more important. The measures for drought forecasting and related contingency besides mitigation planning depend on the quality and quantity of the precipitation data with fine spatiotemporal resolution [11–13]. In the past, the severity of droughts was determined by ground-based observations at specific locations or by estimating the amount of precipitation over a grid with a predetermined scale using various interpolation techniques [14].

Nevertheless, there are several disadvantages in utilizing ground-based observations. In general, drought results from a persistent shortage of precipitation relative to the long-term mean precipitation. Thus, efficient drought monitoring requires long-term data records, yet data from rain gauges are spatially and temporally scattered across developing countries [15]. An alternate source of precipitation data for hydrologic prediction that can address the space–time resolution shortcomings of in situ networks is by adopting satellite-based precipitation products [16]. By improving the temporal and spatial characteristics of the precipitation data, satellite-based products and related global climate models can aid in drought monitoring and other related applications i.e., hydrological modelling [17–20], spatial soil predictions [21,22], and flood forecasting [23,24]. Commonly used precipitation products utilized in the previous studies were IMERG (integrated multi-satellite retrievals for GPM) [25], CHIRPS (climate hazards group infrared precipitation with stations) [26,27], TMPA (TRMM multi-satellite precipitation analysis) [28], CMORPH (CPC morphing technique) [29], MIRAA (microwave/infrared rain rate algorithm) [30], and PERSIANN (precipitation estimation from remote sensing information using artificial neural network) [31]. Previous studies on studying the effectiveness of satellite precipitation products indicated the efficacy of the products over ground observations [32–38]. Derin et al. [39] evaluated nine high-resolution global-scale satellite-based precipitation products over ten regions, including the western Black Sea Region in Turkey, and concluded that many satellite-based precipitation products typically overestimate the dry season precipitation and underestimate the wet season precipitation.

Similarly, for the years 1981 to 2014, Bai et al. [40] assessed the daily CHIRPS product pattern across ten areas in China. They observed that the CHIRPS performed poorly in arid and semi-arid regions. On the other hand, according to Zhu et al. [41], the last run of the IMERG V05 product performed well in estimating short-term drought (2015–2017) over the Xiang River Basin in China. For the monsoon season over India, Prakash and Gairola [42] validated TRMM3B42 (V7 and RT) and global satellite mapping of precipitation (GSMaP) against gauge-based IMD precipitation. For large-scale monsoon rainfall, these two datasets were found to perform well; nevertheless, regional estimates were obtained with bias. Except for orographic areas such as the Northwest and Northeast Himalayan region and Southern peninsular India, it was shown that both types of TRMM datasets overestimated rainfall over the majority of India.

Various drought indices, such as the standardized soil moisture index (SSI) [43], the standardized precipitation evapotranspiration index (SPEI) [44], the vegetation drought response index (Veg-DRI) [45], and the standardized precipitation index (SPI), can be used

to characterize drought [46]. SPI, also known as a meteorological drought index, is one of the most widely used indices for monitoring drought conditions [47]. SPI is considered for its applicability and practical implications over time periods (3, 6, or 12 months). Several studies compared the effectiveness of SPI-based drought monitoring to that of other indices in various climatic locations [48–54]. They resulted in increased efficiency of SPI over other indices in detecting drought incidents. A drought "event" is said to begin when SPI falls below a specific threshold and to end when SPI exceeds the threshold. Therefore, a longer drought period results in fewer drought occurrences. According to a study where classifications made based on NDVI, NDWI, and SPI in the Nammakal district of Tamil Nadu state, the overall extent where drought vulnerability prevailed was at its maximum for the year 2016, which was in accordance with rainfall [55]. From 2000 to 2016, in Tamil Nadu state, an integrated drought monitoring index (IDMI) was developed as a tool to analyse and monitor the spatio-temporal dynamics of agricultural drought during the northeast monsoon season. According to the study, the state of Tamil Nadu had extreme and severe drought conditions in 2016 in proportions of 44.4 and 17.8%, respectively [56]. Research found that the rainfall-based component TRMM had the strongest correlation with rainfall (0.58) and SPI (0.43) for the Tamil Nadu area from 2000 to 2013, offering an alternative option in the absence of in situ meteorological data [57]. A study was conducted in the Kodavanar watershed of Tamil Nadu, displaying signs of drought such as low rainfall and vegetation stress, employing the Google Earth Engine (GEE) platform, which provides comprehensive and effective monitoring of drought events in real time. Land surface temperature (LST), temperature condition index (TCI), normalized difference vegetation index (NDVI), vegetation condition index (VCI), and vegetation health index (VHI) are remote sensing indicators used for agriculture drought evaluation [58].

Adequate climatological data are crucial for assessing drought characteristics. Obtaining long-term meteorological data from ground stations is a significant challenge in developing nations such as India, which suffers from a lack of extent and quality of climatological data from ground stations. As a result, it is necessary to improve resources and approaches for studying and monitoring the various drought characteristics. The northeast monsoon in Tamil Nadu is extremely sensitive to severe drought episodes; therefore, understanding the strengths and weaknesses of various rainfall products is crucial. The purpose of this study was to evaluate the accuracy of remotely sensed precipitation products in Tamil Nadu and their implications for specific purpose in drought detection and monitoring. With these considerations in view, the study was conducted to investigate the reliability and potential of using high resolution precipitation products along with ground-based observation and assessing the intensity of meteorological drought using rainfall departure and standard precipitation index during the northeast monsoon season.

2. Materials

2.1. Study Area

Tamil Nadu has a land area of 13 million hectares and a coastline of 1076 km, accounting for approximately 15% of India's coastline. Tamil Nadu State is in the southernmost part of India's peninsular region, between 08°05′ and 13°35′ Northern Latitudes and 76°15′ to 80°20′ Eastern Longitudes (Figure 1). The Western Ghat mountain ranges run along the state's western border, and the Eastern Ghats are a line of discontinuous hills in the state's northern parts. The plateau lies between the Western and Eastern Ghats, with elevations ranging from 45 to 150 m above mean sea level as the land slopes eastward. The Western Ghats occupy the entire western border with Kerala, essentially keeping much of the South West Monsoon's rain-bearing clouds from entering the state. The state receives the most rainfall from the northeast monsoon than South West Monsoon since the state is located in the Western Ghats rain shadow region. Arid plains dominate the central and south-central areas. The western, southern, and north-western regions are hills, with a combination of vegetation and aridity. Due to its reliance on monsoon rainfall, Tamil Nadu is vulnerable to droughts. The state has a wide range of climates, from semi-arid to wet rainforests.

The state has various rainfall periods, which include the advance monsoon period, the south-west monsoon from June to September with strong southwest winds, the north-east monsoon from October to December with dominant northeast winds, and the dry season from January to May. The state's maximum annual average temperature is around 33 °C, rising to 45 °C in the summer. Excluding the hilly areas, the minimum annual average temperature is 24 °C and drops to approximately 10 °C during the winter. Throughout the year, temperatures and humidity remain relatively high. The annual precipitation of the state reaches an average of 945.9 mm. The rainfall in winter (January–February), summer (March–May), south west monsoon (June–September), and northeast monsoon (October–December) seasons varies and approximately accounts about 3.4, 13.9, 34.9, and 47.8 percent of total rainfall, respectively. Tamil Nadu has seven agro-climatic zones: north-eastern (NEZ), north western (NWZ), western (WZ), high altitude and hilly (HAHZ), Cauvery delta (CDZ), southern (SZ), and high rainfall zones (HRZ). Furthermore, changes in the spatial and temporal distribution of rainfall exacerbate distress in the state's cropping pattern and intensity.
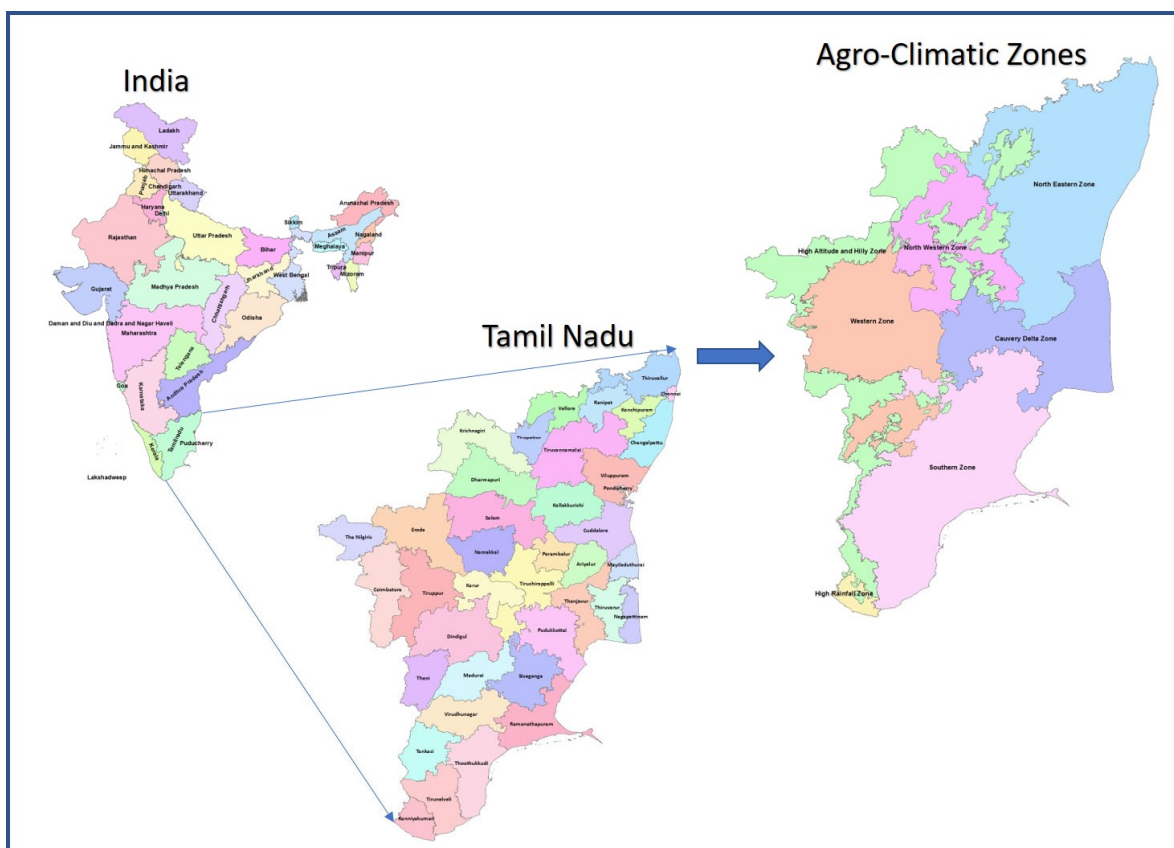

Figure 1. The study area of Tamil Nadu with seven agro-climatic zones.

2.2. Data Collection

The datasets used in the study were downloaded between October 2015 and December 2017, corresponding to Julian days 273 to 353. The rainfall data utilized in the study were collected from rain gauge-based weather stations and satellite precipitation products. The observations were used to assess the performance of remote sensing-based drought indices from 2015 to 2017. The research focused on the northeast monsoon season, which had a significant impact on drought in most parts of Tamil Nadu State.

2.3. Satellite-Based Precipitation Products

This study used four high-resolution satellite rainfall products—TRMM, GPM IMERGM, CHIRPS, and PERSIANN—to compare and assess their accuracy against observations

from rain gauges. The product attributes and algorithm structures were also employed from October to December between 2015 and 2017. Table 1 provides an overview of the chosen products and a succinct description. The study period was limited from October to December (northeast monsoon) due to the increased precipitation rates. Furthermore, rainfall products were selected due to their relatively high spatial resolution, long series, availability, and applicability.

Table 1. Overview of satellite-based precipitation products.

Data Set	Developing Agency	Coverage	Period	Spatial Resolution	Temporal Resolution
CHIRPS Version 2.0	United States Geological Survey (USGS) and the Climate Hazards Group at the University of California	Quasi-global coverage of 50° S–50° N, 180° E–180° W	1981–present	0.25° (~27 km)	Daily
TRMM 3B42 V. 7	National Aeronautics and Space Administration (NASA) and Japan Aerospace Exploration Agency	Global 50° N–S	1998–present	0.25° (~27 km)	Daily
PERSIANN	Center for Hydrometeorology and Remote Sensing (CHRS) at the University of California, Irvine	Global 60° N–S	2000–present	0.25° (~27 km)	Daily
GPM 3IMERGF Version 05	National Aeronautics and Space Administration (NASA) and Japan Aerospace Exploration Agency	Quasi global coverage	2014–present	0.01° (~10 km)	Daily

2.3.1. Global Precipitation Measurement (GPM) Integrated Multi-Satellite Retrievals for GPM (GPM IMERG)

The GPM mission employs a constellation of satellites from several providers and a primary satellite calibration to collect data in near real-time on as many passive microwave (PMW) and infrared (IR) platforms as possible. A combined PMW-IR technique may increase the value of individual PMW or IR satellite rainfall estimations. When the PMW and IR platform observation data are received, is the data are merged into half-hour grid fields using the integrated multi-satellite GPM retrieval system (IMERG) [25]. It comprises one core observatory satellite and around ten constellation satellites. GPM products are available in multiple levels and versions. Levels 1–3 depict the various steps of satellite data processing, where the third level represents the final processed precipitation product. This study downloaded data from the final run of 2015 to 2017 daily GPM 3IMERGF version 05. IMERG data were provided by NASA/Goddard Space Flight Center PMM [59] and accumulated on a monthly time scale. The latest V05 version of the IMERG Final Run product, available since March 2014, was used in the study.

2.3.2. Tropical Rainfall Measurement Mission (TRMM)

The tropical rainfall measurement mission monitors tropical/subtropical precipitation with 0.25° spatial resolution; the monthly and daily accumulations of 3 h TMPA are the most extensively used outputs (TRMM 3B42). The TRMM satellite featured five instruments: the visible infrared radiometer (VIRS), the TRMM microwave imager (TMI), the precipitation radar (PR), the cloud and Earth radiant energy sensor (CERES), and the lightning imaging sensor (LIS) [28,60]. The TRMM satellite's rainfall measuring instruments includes TRMM microwave image (TMI) from a nine-channel passive microwave radiometer that gives information on the integrated column precipitation content, cloud liquid water, cloud

ice, rain intensity, and rainfall types. The global precipitation climatology center (GPCC) generates a level 3 product, 3B43, using the TRMM-based Huffman algorithm [61,62]. The TRMM 3B43 version 7 merged daily product (TMPA) dataset for northeast monsoons from 2015 to 2017 used in the study was obtained from the Goddard Active Archive Center (DAAC).

2.3.3. Climate Hazards Group Infrared Precipitation and Stations (CHIRPS)

CHIRPS is a blended product with the following data sources: (i) pentad grid-scale precipitation climatology (six pentads per month); (ii) quasi-global geostationary thermal infrared (IR) satellite observations from the Climate Prediction Center (CPC) and the National Climatic Data Center (NCDC) (B1 IR); (iii) NASA's tropical rainfall measuring mission (TRMM) 3B42 product; (iv) atmospheric data center (B1 IR). All data sources were compiled using five-day rainfall accumulations and in situ precipitation measurements received from several sources, including national and regional meteorological agencies [26]. For 2015–2017, the CHIRPS product was used with a monthly aggregation covering the period of ground rainfall data. The monthly scale was chosen because it is ideal for drought monitoring using drought indices such as the standardized precipitation index [63] and environmental monitoring [64]. For the study, daily CHIRPS v2.0 data from 2015 to 2017 were collected and aggregated spatially to a resolution of 0.25° and accumulated to a monthly time scale [65].

2.3.4. Precipitation Estimation from Remotely Sensed Information using Artificial Neural Networks (PERSIANN)

The PERSIANN precipitation product system contains an adaptive training feature that updates network parameters whenever independent rainfall estimates are available. The PERSIANN family includes three satellite estimation products: PERSIANN, PERSIANN-Cloud Classification System (CCS), and PERSIANN-Climate Data Record (CDR). The PERSIANN algorithm is a multilayer neural feed-forward network (ANN) model established in 1997, based on a multilayer neural feed-forward network (MFN) known as the modified counter propagation network [31] and synergy between low-earth orbiting (LEO) satellite information samples and high-frequency samples from geostationary (GEO) satellites [31,66]. This hybrid model is made up of two processes. First, the infrared (10.2–11.2 m) images are transformed into the hidden layer using an automated clustering procedure, resulting in a self-organizing feature map (SOFM). For the study, the daily PERSIANN data from 2015 to 2017 during the northeast monsoon were derived from the CHRS website and accumulated on a monthly time scale.

2.4. In-Situ Rain Gauge Data

The network of Tamil Nadu Automatic Weather Stations (AWS) rain gauges of the Agro Climate Research Centre at the Tamil Nadu Agricultural University provided the surface rain gauge measurement of observed daily rainfall data for the 391 stations for northeast monsoon periods from 2015 to 2017. The ground observation network comprised 385 tipping-bucket rain gauges with a 25 km spatial resolution. Figure 2 shows the geographical distribution of AWS gauge stations over Tamil Nadu. For 37 years, from 1980 to 2017, the historical daily rainfall data were obtained from the State Ground and Surface Water Resources Data Centre, Water Resources Department, Tamil Nadu, and were used for meteorological drought analysis. The ground observations were then spatially interpolated through the kriging method to identify the spatial distribution of the rain gauge data. The kriging method was then used to interpolate the rain gauge data into the spatial distribution. CHIRPS satellite precipitation data were validated for rainfall deviation analysis using December 2017 rainfall data.
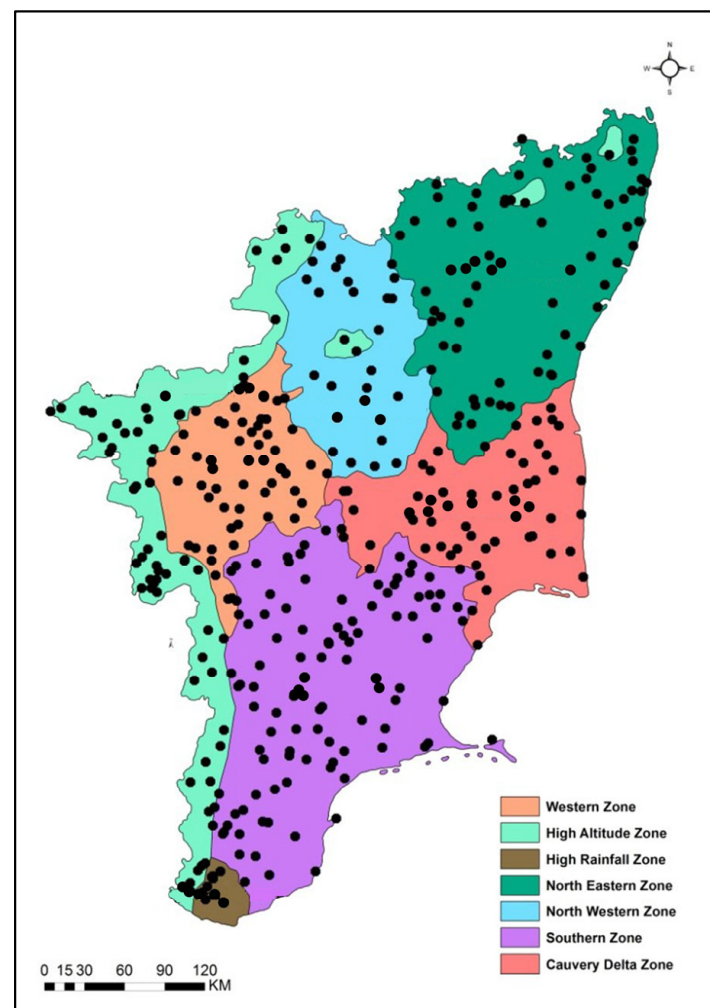
Figure 2. In-situ rain gauge distribution in different zones of Tamil Nadu.

3. Methodology

3.1. Evaluation of High-Resolution Precipitation Products

This study validated the satellite rainfall products for the northeast monsoon season from 2015 to 2017 using data from 391 independent weather stations in Tamil Nadu. The selection of independent weather stations was facilitated based on the relative location of each station in different agro-climate zones and the availability of good records. Most satellite rainfall products blend data from ground-based weather stations to improve their accuracy and reliability. Therefore, validation with an independent data set is crucial in the study region to identify the best satellite product to supplement reproduction gauge observations to reproduce the measured data.

Satellite rainfall products were evaluated at monthly and seasonal time scales by accumulating daily rainfall data. Analysis to validate the satellite precipitation product retrievals with gauge data was carried out point-to-point for all seasonal and monthly series meteorological stations. Since rainfall measurements are taken from a rain gauge network, an interpolation scheme was used to obtain rainfall from the scattered point values. The ordinary kriging method was used for interpolating the rain gauge measurements. All the maps and figures were analysed using ArcGIS 10.6 and the R-Programming interface 1.1.419 (Figure 3).
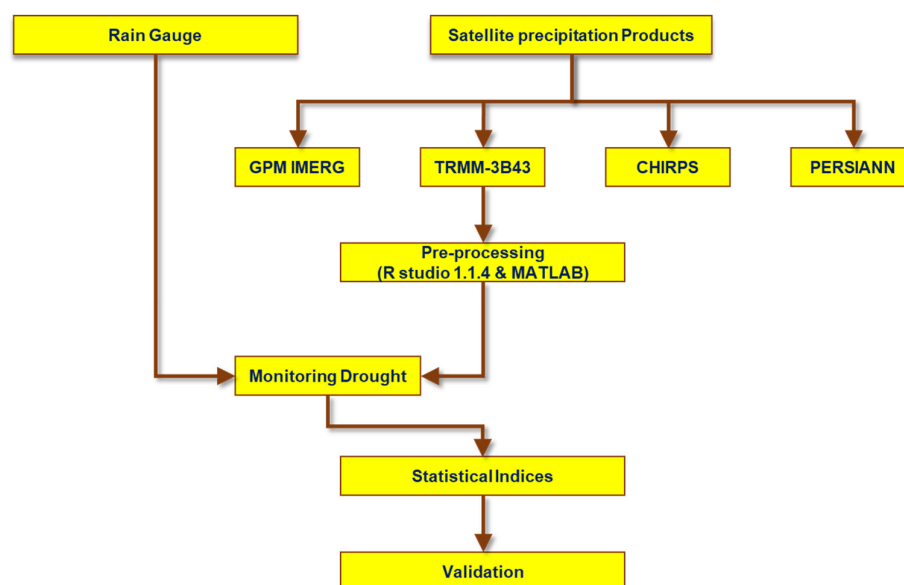
Figure 3. Methodology for validation of satellite precipitation products.

3.2. Performance Metrics

The Pairwise comparison statistics techniques such as Pearson's correlation coefficient (CC), root mean square error (RMSE), normalized root mean square error (NRMSE) and agreement (Table 2) were used for quantitative validation of the satellite rainfall estimates for each set of verification data. Rainfall statistics were calculated monthly and seasonally, and all analyses were performed in the R environment (RStudio) version 1.1.463.

Table 2. Performance metrics used in this study to evaluate the satellite precipitation products.

Metric	Equation	Interpretation	Reference
Pearson Correlation Coefficient	$CC = \dfrac{\sum_{i=1}^{N}(HRPP_i - \overline{HRPP}) \cdot (AWS_i - \overline{AWS})}{\sum_{i=1}^{N}(HRPP_i - \overline{HRPP})^2 \cdot (AWS_i - \overline{AWS})^2}$	The value ranges between −1 to 1, in which one indicates the perfect score.	[50]
Root Mean Square Error (RMSE)	$RMSE = \sqrt{\dfrac{1}{n}\sum_{i=1}^{n}\left(\dfrac{AWS_i - HRPP_i}{N}\right)^2}$	A lower RMSE value means greater central tendencies and small extreme errors. The zero RMSE value is the perfect score.	[50]
Normalized Root-Mean-Square Error (NRMSE)	$NRMSE = 100 \times (RMSE/Oi)$	Lower NRMSE values indicate less residual variance for a model.	[67]
Agreement (%)	$Agreement\,(\%) = 100 \times (1 - (RMSE/Oi))$	Closer values to 100% indicate strong agreement, and values closer to 0% indicate the least agreement.	[68]

Note: AWSi = gauge rainfall measurement, $\overline{AWS}$ = average gauge rainfall measurement, HRPPi = satellite rainfall estimate, $\overline{HRPP}$ = average satellite rainfall estimate, Oi = Observed value, and N = number of data pairs.

3.3. Calculation of Standardized Precipitation Index (SPI)

The standardized precipitation index (SPI) [46] is a multivariate meteorological drought index based on the probability distribution of precipitation. SPI values are dimensionless and are computed by fitting a Gamma distribution function to precipitation values during the time (month) period. In this study, SPI was computed with 1-month accumulation interval. It provided an easy and flexible way to monitor drought on a different scale, showing wetness and dryness conditions for any specified location based on the long-term record for the desired precipitation period. Table 3 presents the categories of the event corresponding to SPI values. The SPI represents the total difference in precipitation over a

given period from its climatological mean and is then normalized by the standard deviation of precipitation over the same period using the formulae:

$$SPI = a - A/Sd$$

where a = current precipitation for a given period (week, month), A = long-term normal of precipitation for the same period, and Sd represent the standard deviation of precipitation for the given period.

Table 3. Event Classification Based on SPI Values.

SPI Value	Category	Probability (%)
>2.00	Extremely wet	2.3
1.50–1.99	Severely wet	4.4
1.00–1.49	Moderately wet	9.2
−0.99 to 0.99	Near normal	68.2
−1.00 to −1.49	Moderately dry	9.2
−1.50 to −1.99	Severe dry	4.4
<−2.0	Extremely dry	2.3

Positive SPI values are greater than average precipitation, and negative values are less than average precipitation. Depending on the SPI, the drought begins when the SPI value is equal to or below −1, 0 and ends when the value is positive (Table 3, Figure 4). Daily precipitation data were cleaned and aggregated into monthly data for the study periods to calculate the SPI values.
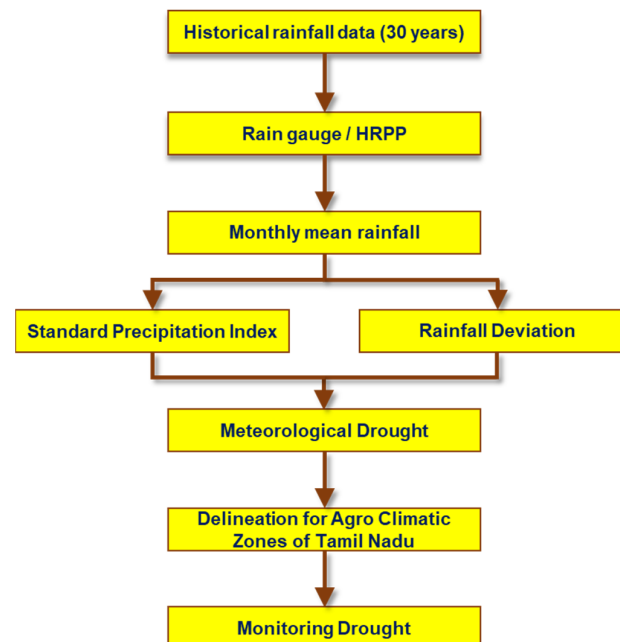
Figure 4. Flow diagram showing the development of drought monitoring system.

The short-term SPI calculation for any location was based on the long-term precipitation record for a desired period because it provided short-term soil moisture and crop stress (especially during the growing season). Therefore, 37 years preceding 2017 (generally 1980–2017) were analysed for each station, and then, the function was standardized to obtain the SPI value.

It could be said that the z-score of the distribution function represents the deviation event from the rainfall data mean as the SPI value. The missing records were excluded, and a total of 550 stations were used for the spatial interpolation of the SPI values using the Spline method. The calculated SPI values were then classified according to the range and probability per cent represented in Tables 3 and 4. This long-term record was equipped with a distribution of probability, which was then converted into a normal distribution so that the mean SPI for the desired time and location was zero. A drought event begins when the SPI value reaches −1.0 and ends when SPI becomes positive again. Since drought is a regional phenomenon, SPI values of the rain gauge stations were interpolated using the Spline interpolation technique in ArcGIS to demarcate its spatial extent. The SPIRITS software was used to generate SPI images for anomaly assessment.

Table 4. Drought intensity based on the percentage departure of rainfall from the normal value given by IMD, 1971.

Percentage Rainfall Deviation	Rainfall Deviation Category	Intensity of Drought
60 and more	Large Excess	No drought
20 to 59	Excess	No drought
+19 to −19	Normal	Mild drought
−59 to −20	Deficient	Moderate drought
−99 to −60	Large Deficient	Severe drought
−100	No Rain	Extreme drought

3.4. Calculation of Rainfall Deviation

The monthly drought condition was determined using the criteria suggested by IMD [69]. It was based on the percentage deviation of rainfall from its long-term mean. According to the India Meteorological Department (IMD), meteorological drought is the deviation of actual rainfall from long-term average (normal) records at a given station. It is calculated using the following formula;

$$Rfdev = [(Rfi - RFn)/RFn] \times 100$$

where Rfi is the current rainfall for a comparable period (in mm), and RFn is the normal rainfall (at least 30 years on average) for the same period (in mm). Based on rainfall deviations, four categories are used to monitor and evaluate rainfall patterns across Tamil Nadu during the north-eastern monsoon season. The rainfall deviation classification of IMD is given in Table 4 and Figure 4.

4. Results

Four high-resolution precipitation products, IMERGH, TRMM, CHIRPS, and PER-SIANN, were evaluated for accuracy and confidence level with AWS network data to determine the usability and applicability of global precipitation products as alternatives to ground-based rainfall estimation. In addition, estimates of the global precipitation products based on agroclimatic zones were investigated to comprehend rainfall distribution and its influence on ACZs.

4.1. Spatial Distribution of Precipitation Products and AWS Data

The spatial distribution of accumulated precipitation was derived from the high-resolution precipitation products IMERGH, TRMM, CHIRPS, and PERSIANN, and from the AWS stations of Tamil Nadu; all of which are depicted in Figure 5. IMERGH recorded a minimum of 149.75, 32.07, and 80.05 mm during the northeast monsoon of 2015, 2016, and 2017, respectively. The corresponding maximum values were 1453.63, 253.40, and 700.59 mm, respectively. A minimum precipitation of 144.31, 34.40, and 75.01 mm were

recorded with TRMM during the northeast monsoon of 2015, 2016, and 2017, respectively. Maximum values of 1400.07, 250.98, and 686.95 mm were recorded in the corresponding years. Accumulated precipitation data with CHIRPS recorded a minimum of 296.34, 95.24, and 171.65 mm during the northeast monsoon of 2015, 2016, and 2017, respectively. The corresponding maximum values were 1563.72, 421.12, and 722.88 mm, respectively. During the northeast monsoon of 2015, 2016, and 2017, PERSIANN recorded minimum precipitation of 219.87, 59.83, and 171.65 mm and maximum precipitation values of 1411.29, 243.87, and 722.88 mm in the respective years. AWS recorded a minimum of 151.65, 31.82, and 73.29 mm during the northeast monsoon of 2015, 2016, and 2017, respectively. Maximum values of 1755.31, 450.39, and 939.58 mm were recorded in the corresponding years.
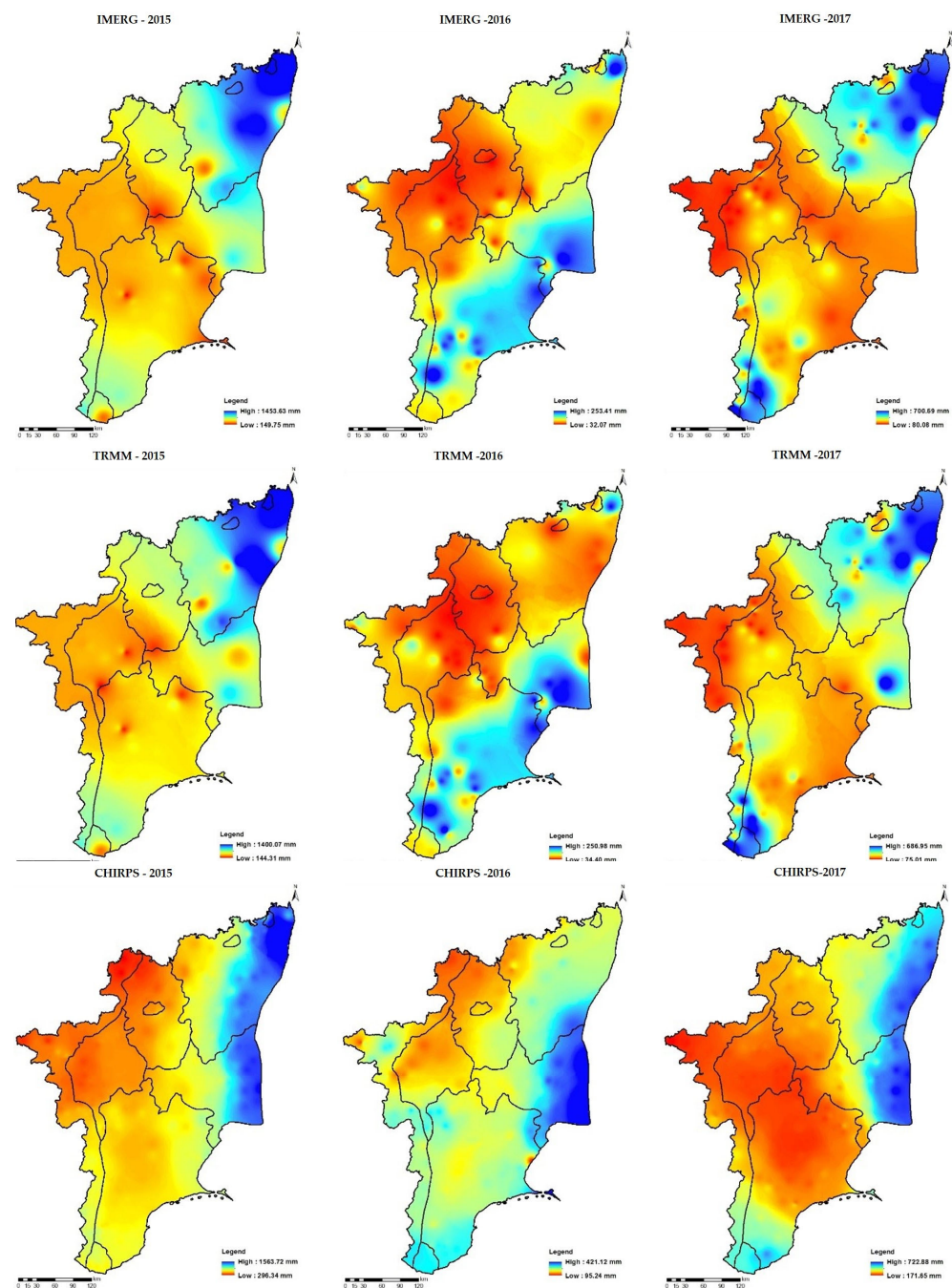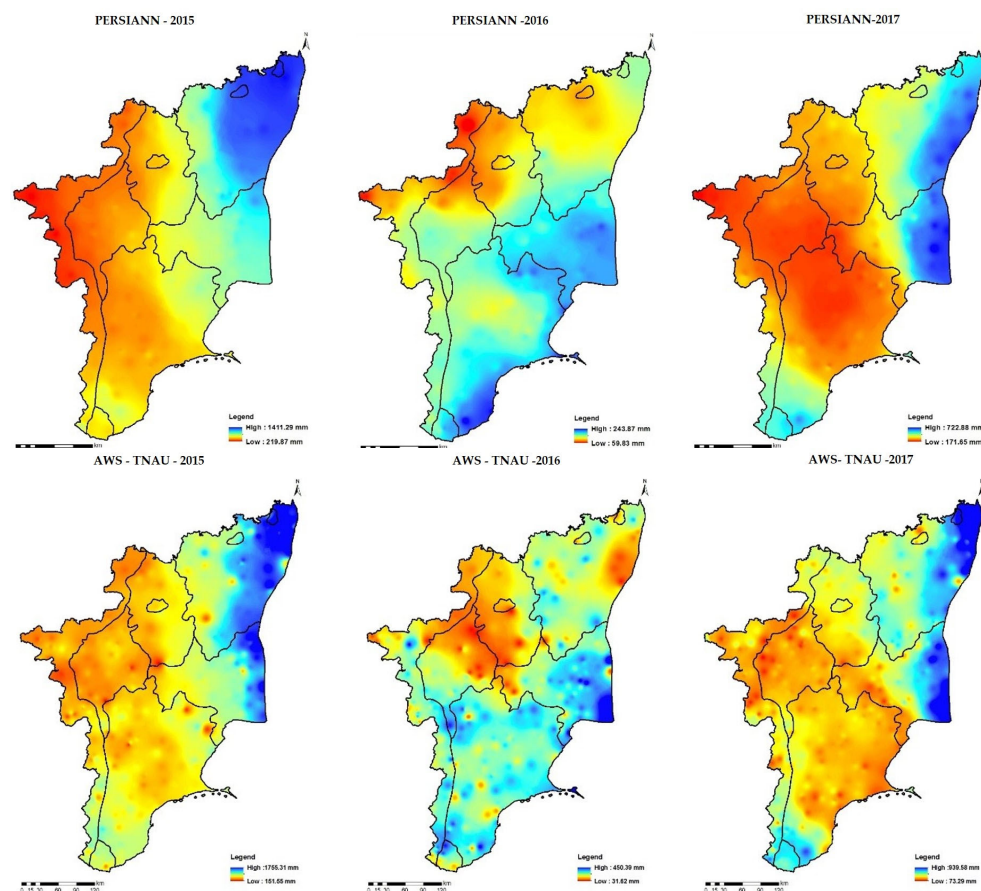

Figure 5. *Cont.*

Figure 5. Spatial distribution of accumulated precipitation for IMERGH, TRMM, CHIRPS, PERSIANN, and AWS-TNAU products during NEM between 2015 and 2017.

During 2015, IMERGH, TRMM, CHIRPS, and PERSIANN recorded the maximum values of 1453.63, 1400.07, 1563.72, and 1411.29 mm of precipitation, respectively, as against 1755.31 mm recorded with AWS. Minimum precipitation of 149.5, 144.31, 296.34, and 219.87 mm was recorded with the respective high-resolution precipitation products, and AWS recorded 151.65 mm precipitation, contrary to the precipitation products. IMERGH, TRMM, CHIRPS, and PERSIANN recorded the maximum values of 253.40, 250.98, 421.12, and 243.87 mm of precipitation, respectively, during 2016, as against 450.39 mm recorded with AWS. Minimum values of 32.07, 34.40, 95.24, and 59.83 mm of accumulated precipitation were recorded with the corresponding satellite precipitation product in contrast with AWS, which recorded 31.82 mm of precipitation. During 2017, the maximum precipitation values of 700.59, 686.95, 722.88, and 722.88 mm were recorded with IMERGH, TRMM, CHIRPS, and PERSIANN, respectively, when compared with 939.58 mm precipitation recorded in AWS. Minimum precipitation of 80.05, 75.01, 171.65, and 171.65 mm was recorded with the respective precipitation products, and AWS recorded 73.29 mm of precipitation uncontrived to the high-resolution precipitation products.

4.2. Seasonal Precipitation Evaluation of Four High Resolution Precipitation Products

Comparing the precipitation products with that of AWS was facilitated through the computation of CC, RMSE, NRMSE, and Per Cent Agreement (Table 5 and Figure 6). From the assessed statistical measures, the correlation coefficient (CC) ranged from 0.77 to 0.85, and the highest CC of 0.85 was observed with IMERGH, followed by TRMM (0.84) and CHIRPS (0.78). The lowest CC of 0.77 was observed with PERSIANN in 2015. During NEM 2016, TRMM and IMERGH recorded higher values for CC i.e., 0.85 and 0.84, respectively, followed by PERSIANN (0.53). During the drought year of 2016, CHIRPS registered the lowest CC of 0.45 among the satellite precipitation products compared to AWS data. Similar

to 2015, IMERGH recorded higher CC of 0.861, followed by TRMM (0.86) and CHIRPS (0.753) during NEM 2017. The least CC of 0.712 was observed with PERSIANN. The seasonal RMSE recorded the least for IMERGH, with a value of 58.49 mm, followed by TRMM, which recorded an RMSE of 96.57 mm. CHIRPS and PERSIANN were in the lower order with RMSE of 127.4 and 134.73 mm during the northeast monsoon of 2015. In the case of northeast monsoon of 2016, TRMM registered the lowest RMSE of 17.47 mm, followed by IMERGH (19.11 mm), whereas CHIRPS recorded the highest RMSE of 43.13 mm next to PERSIANN (29.83 mm). Similarly, TRMM and IMERGH registered comparatively lesser RMSE during northeast monsoon 2017 with values of 44.52 and 45.09, followed by PERSIANN and CHIRPS with higher values of 69.51 and 81.29 mm of RMSE.

Table 5. NEM statistical evaluation of satellite precipitation products during 2015–2017.

Northeast Monsoon 2015				
Index	IMERGH	TRMM	CHIRPS	PERSIANN
CC	0.853	0.835	0.781	0.77
RMSE	58.49	96.57	127.24	134.73
NRMSE	10.24	17.46	18.05	18.88
Agreement	89.76	82.54	81.95	81.12
Northeast Monsoon 2016				
Index	IMERGH	TRMM	CHIRPS	PERSIANN
CC	0.844	0.854	0.449	0.525
RMSE	19.11	17.47	43.13	29.83
NRMSE	19.01	17.75	20.53	19.42
Agreement	80.99	82.25	79.47	80.58
Northeast Monsoon 2017				
Index	IMERGH	TRMM	CHIRPS	PERSIANN
CC	0.861	0.86	0.753	0.712
RMSE	45.09	44.52	81.29	69.51
NRMSE	19.05	19.32	18.63	19.07
Agreement	80.95	80.68	81.37	80.93

Note: CC: Correlation Coefficient; RMSE: Root Mean Square Error; NRMSE: Normalized Root Mean Square Error.

4.3. Accuracy Assessment of High-Resolution Satellite Precipitation Products at the Regional Scale

The agreement between the high-resolution precipitation and the data collected from AWS was determined to evaluate the performance of the precipitation products to ground reality. The results of correlation coefficient (R2), RMSE, and NRMSE were derived for the products during the northeast monsoon season of 2015, 2016, and 2017 in seven agro-climatic zones of Tamil Nadu (Table 6). Irrespective of the agro-climatic zones, the R^2 value for IMERGH during NEM 2015 was more than 0.8 except for high altitude and hilly Zones (0.68), which revealed that the IMERGH product performance was high and dependable for use. Even though RMSE values were high in HAHZ and NEZ and the other zones recorded less value, the agreement of the data with AWS values was more than 74 per cent indicating the high correlation of the data with ground truth. Similar results of the agreement were found for all the other precipitation products with more than 70 per cent. TRMM data were found to have higher R^2 values of more than 0.6 in all the northeast monsoon seasons of 2015, 2016, and 2017, irrespective of the agro-climatic zones assessed.
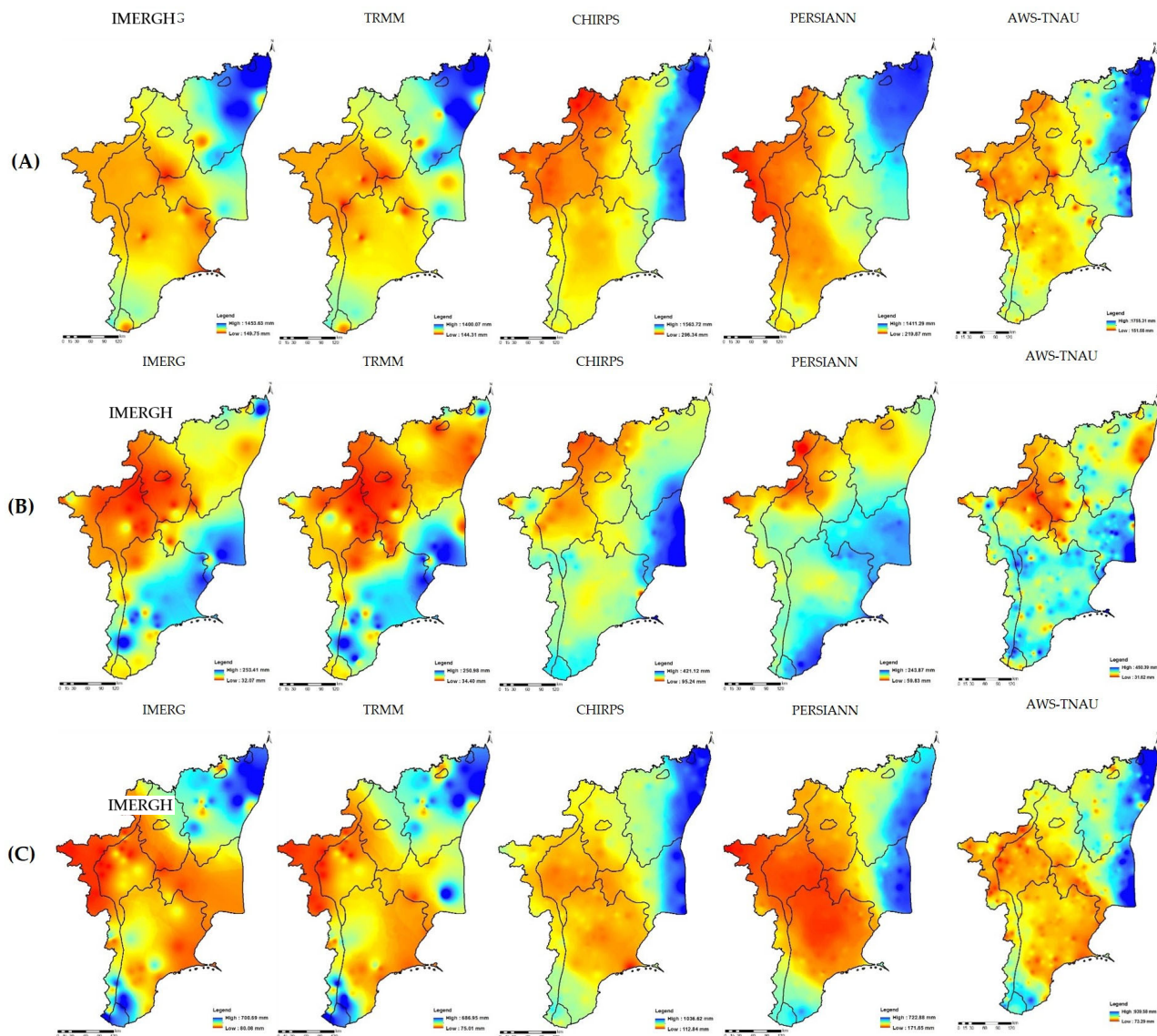
Figure 6. Spatial distribution of seasonal precipitation of high-resolution precipitation products during (**A**) 2015, (**B**) 2016, and (**C**) 2017 from interpolated gauge station at the spatial resolution of 0.25 degree.

It was found that the CHIRPS and PERSIANN products had a high variation in the R^2 value, indicating the inconsistency of predicted precipitation over different agro-climatic zones. For example, the R^2 value was as low as 0.1 and 0.22 in HRZ during 2015 for PERSIANN and CHIRPS data, respectively. Similarly, the PERSIANN data recorded very low R^2 values irrespective of the years and agro-climatic zones analysed and a high RMSE in most of the zones, which affirmed the less predictable precipitation product compared to the other three products under evaluation. Further, PERSIANN is a pure satellite precipitation product based on the artificial neural network (ANN) model by the Centre for Hydrometeorology and Remote Sensing (CHRS) of California. Therefore, the product depends on the statistical relationship between IR and the precipitation rate exhibiting considerable uncertainty [66].

Table 6. Values of the R^2, RMSE, NRMSE, and Agreement of seasonal evaluation of high-resolution precipitation products for the seven agro-climatic zones.

	Northeast Monsoon 2015				Northeast Monsoon 2016				Northeast Monsoon 2017			
Cauvery Delta Zone (CDZ)												
Index	**IMERGH**	**TRMM**	**CHIRPS**	**PER-SIANN**	**IMERGH**	**TRMM**	**CHIRPS**	**PER-SIANN**	**IMERGH**	**TRMM**	**CHIRPS**	**PER-SIANN**
CC	0.99	0.71	0.92	0.69	0.87	0.86	0.83	0.25	0.82	0.82	0.95	0.71
RMSE	36.85	78.59	77.05	93.33	18.04	17.19	28.05	33.38	49.18	46.02	55.04	85.04
NRMSE	23.26	16.62	25.19	10.57	17.68	14.00	10.49	18.15	19.73	21.04	10.44	18.80
Agreement	76.74	83.38	74.81	89.43	82.32	86.00	89.51	81.85	80.27	78.96	89.56	81.20
High Altitude and Hilly Zone (HAHZ)												
CC	0.68	0.67	0.89	0.79	0.72	0.73	0.75	0.56	0.92	0.92	0.89	0.70
RMSE	129.43	136.24	53.93	75.60	21.98	20.84	21.95	22.63	38.48	37.94	34.71	55.52
NRMSE	25.52	28.33	9.63	16.79	20.04	18.80	11.16	18.82	16.03	18.10	8.20	19.40
Agreement	74.48	71.67	90.37	83.21	79.96	81.20	88.84	81.18	83.97	81.90	91.80	80.60
High Rainfall Zone (HRZ)												
CC	0.98	0.96	0.22	0.10	0.60	0.70	0.81	0.45	0.34	0.34	0.71	0.59
RMSE	21.16	43.61	59.15	139.17	27.62	26.43	25.72	38.62	67.75	64.76	46.13	124.01
NRMSE	16.39	23.95	8.37	24.99	22.75	20.89	10.37	20.80	33.55	31.01	9.34	23.15
Agreement	83.61	76.05	91.63	75.01	77.25	79.11	89.63	79.20	66.45	68.99	90.66	76.85
Northeastern Zone (NEZ)												
CC	0.79	0.78	0.83	0.52	0.89	0.93	0.68	0.53	0.83	0.80	0.81	0.47
RMSE	149.40	146.96	80.78	222.17	15.07	11.44	19.63	31.18	62.79	64.59	72.79	104.69
NRMSE	19.43	18.53	8.20	19.45	18.96	17.02	10.58	22.63	18.29	17.67	11.06	21.87
Agreement	80.57	81.47	85.80	80.55	81.04	82.98	89.42	77.37	81.71	82.33	88.94	78.13
North-western Zone (NWZ)												
CC	0.99	0.99	0.80	0.44	0.94	0.92	0.58	0.48	0.70	0.71	0.44	0.40
RMSE	60.25	31.17	49.13	109.30	7.33	8.18	19.44	23.41	60.66	63.27	52.57	50.55
NRMSE	19.63	13.62	10.86	19.73	18.19	20.50	13.57	21.57	31.13	31.42	14.17	17.64
Agreement	80.37	86.38	89.14	80.27	81.81	79.50	86.43	78.43	68.87	68.58	85.83	82.36
Southern Zone (SZ)												
CC	0.86	0.75	0.58	0.35	0.84	0.84	0.64	0.26	0.84	0.86	0.85	0.71
RMSE	75.22	70.15	68.17	106.34	23.49	22.71	20.52	33.07	39.74	37.62	30.88	51.90
NRMSE	14.56	14.07	10.61	18.90	17.37	16.73	9.87	18.69	19.86	19.52	9.10	18.30
Agreement	85.44	85.93	89.39	81.10	82.63	83.27	90.13	81.31	80.14	80.48	90.90	81.70
Western Zone (WZ)												
CC	0.83	0.78	0.68	0.56	0.78	0.80	0.82	0.71	0.86	0.80	0.72	0.30
RMSE	54.53	54.50	51.66	41.74	17.04	14.33	13.29	25.26	22.55	24.33	26.50	32.22
NRMSE	18.18	15.95	11.42	20.45	21.08	19.66	8.02	19.85	13.74	15.30	9.93	14.98
Agreement	81.82	84.05	88.58	85.69	78.92	80.34	89.98	80.15	86.26	84.70	90.07	85.02

Note: CC: Correlation Coefficient; RMSE: Root Mean Square Error; NRMSE: Normalized Root Mean Square Error.

4.4. Drought Assessment Based on the Standardized Precipitation Index

Standardized precipitation index (SPI) computes rainfall deviation from the long-term historical mean for three months, viz., October, November, and December, for different agro-climatic zones of Tamil Nadu during the years 2015 to 2017 and it is presented in Table 7 and Figure 7. It is a known fact that a dry spell occurs when the SPI values are found to be negative, while the non-dry spells are indicated by positive values [70]. Thereby, it could be inferred that the negative values of SPI indicate the drought condition, and positive values affirm the non-drought condition.

Table 7. Agroclimatic zone-wise SPI for different months during 2015–2017.

ACZ	15 October	15 November	15 December	16 October	16 November	16 December	17 October	17 November	17 December
Southern Zone	Mi D	Mi W	Mi W	SD	ED	Mi D	Mi D	Mi D	Mi D
Northeast Zone	Mi D	Mi W	Mi D	ED	ED	Mi D	Mi D	Mi D	Mi D
High Rainfall Zone	MD	N	N	SD	ED	Mi D	MW	Mi D	MW
Cauvery Delta Zone	Mi D	Mi D	Mi D	SD	ED	Mi D	Mi D	Mi D	Mi D
Western Zone	Mi D	SW	MW	SD	ED	Mi D	N	Mi D	N
High Altitude and Hilly Zone	Mi D	SW	SW	SD	ED	Mi D	Mi W	Mi D	Mi W
North-western Zone	Mi D	SW	Mi D	ED	MD	Mi D	N	Mi D	N

Note: Mi D—Mildly dry; Mi W—Mildly wet; MD—Moderately dry; MW—Moderately wet; SW—Severely wet; SD—Severely dry; ED—Extremely dry; N—Normal.

Based on SPI values for October, the high rainfall zone was deemed moderately dry in 2015, while the remaining blocks were found to be mildly dry. During November, the Cauvery delta zone was categorized as mildly dry, while the high rainfall zone was determined to be normal, the southern zone and north-east zone were classified as mildly wet, and the remaining zones were classified as severely wet. For December, the northeast zone, Cauvery delta zone, and north western zone were classified as mildly dry, the high rainfall zone as normal, and the southern zone, western zone, high altitude, and hilly zone as mildly, moderately, and severely wet based on SPI values. During October 2016, the northeast zone and north western zone recorded SPI classes of extremely dry, while the rest zones were classified as severely dry. Except for the north western zone, which was moderately dry in November, the remaining six zones were classified as extremely dry. For December, all the zones were in mildly dry condition. All the zones were classified under mildly dry conditions in October and November 2017. For December, the southern zone, northeast zone and Cauvery delta zone were mildly dry. While the western zone and north western zone were grouped as normal, and high altitude and hilly zone and high rainfall zone registered SPI classes of mildly and moderately wet, respectively, during 2017.

4.5. Assessment of Meteorological Drought Based on Rainfall Departure

According to the India Meteorological Department IMD [39], meteorological drought is the deviation of actual rainfall from long-term average (normal) records at a given station. During 2015, the high rainfall agro-climatic zone was found to have excess rainfall during October, November, and December, and was classified under the no drought category, whereas the other zones of Tamil Nadu fell under the moderate drought category. On the other hand, the rainfall deviation during the northeast monsoon for the years 2016 and 2017 was mostly classified under the deficient and large deficient categories, indicating that the drought severity in Tamil Nadu varied between moderate and severe drought conditions. From the percentage departure, it could be concluded that 2016 and 2017 fell under severe drought and moderate drought conditions, respectively. In contrast, 2015 was observed to have mild drought in the western, high altitude, and hilly and north western zones of Tamil Nadu, and the remaining zones were classified under no drought. The same methodology to identify the drought years was followed by Karinki and Sahoo [71]. Furthermore, the rainfall deviation map was generated for each district to know the district-wise drought severity condition. The number of districts falling into different severity categories is summarized and shown in Table 8.
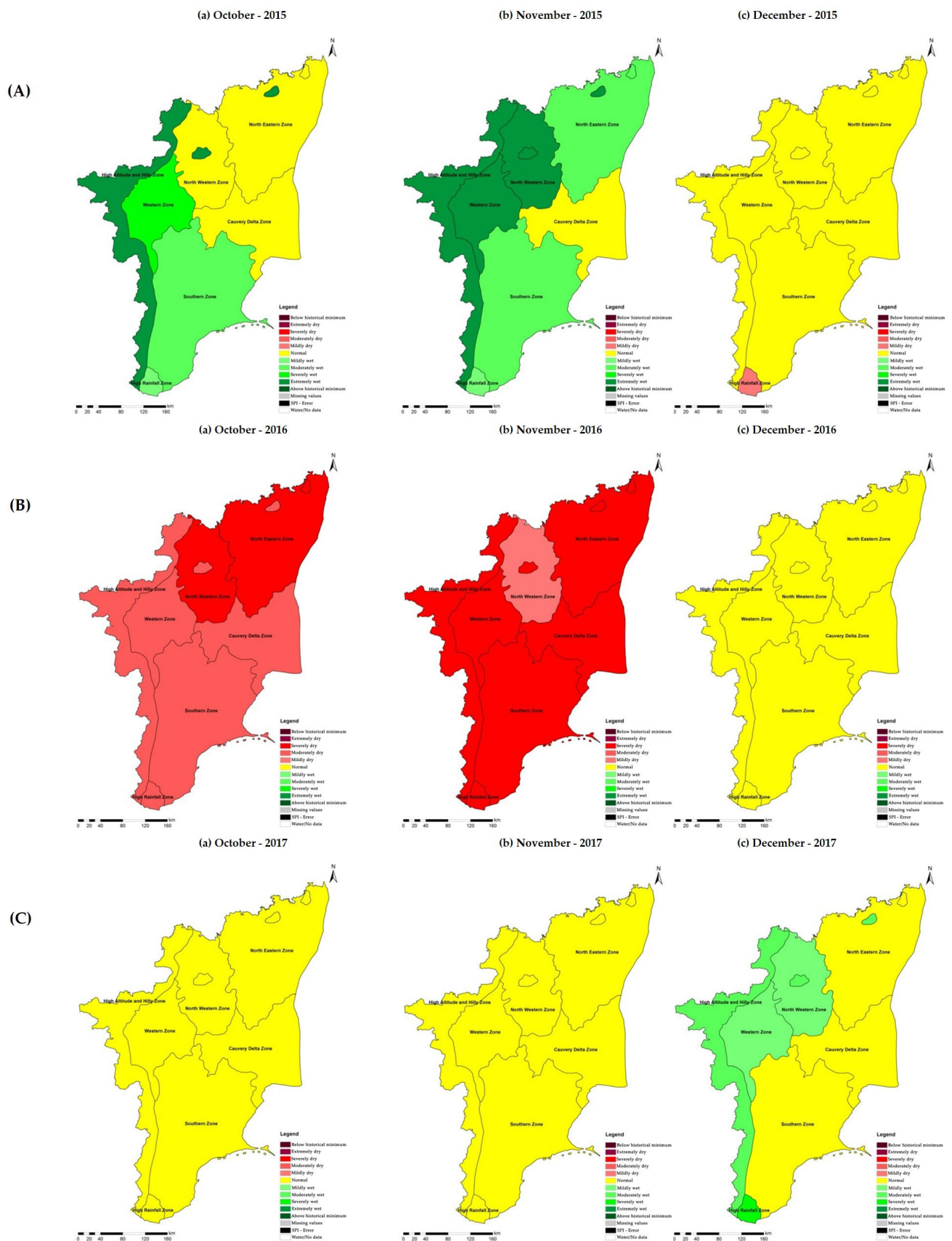
(a) October - 2015   **(b) November - 2015**   **(c) December - 2015**

(A)

(a) October - 2016   **(b) November - 2016**   **(c) December - 2016**

(B)

(a) October - 2017   **(b) November - 2017**   **(c) December - 2017**

(C)

Figure 7. Agro-climatic zone-wise SPI of spatial distribution for rainfall departure during (**A**) 2015, (**B**) 2016, and (**C**) 2017.

Table 8. Summary of the number of districts falling into different severity categories.

Drought Severity Class	Number of Districts								
	15 October	15 November	15 December	16 October	16 November	16 December	17 October	17 November	17 December
No drought	1	31	20	0	0	6	6	3	2
Mild drought	6	1	9	0	0	6	7	8	4
Moderate drought	24	0	3	12	3	15	17	20	18
Severe drought	1	0	0	20	29	5	2	1	8

From Table 8, it could be inferred that during the years 2016 and 2017, most districts were classified under moderate and severe drought conditions. The year 2015 depicted moderate drought conditions prevailing during October, whereas no drought was found during November and December.

5. Discussion

Among the satellite precipitation products evaluated, the range of minimum and maximum values recorded precipitation was similar for IMERGH and TRMM. The other two products, CHIRPS and PERSIANN estimation, were in a higher range during the years. While comparing AWS estimates, IMERGH, and TRMM were on par with the minimum range predictions, the other two products were over-estimated. IMERG, TMPA, and Global Satellite Mapping of Precipitation (GSMaP, v. 6) estimations were compared to gauge-based data over India daily for the southwest monsoon season (June to September 2014) by Prakash et al. [72]. The results showed that the IMERG product performed a clear improvement in missed and false precipitation bias over India, accurately representing the mean monsoon precipitation and its variability. The Monsoon Core Region of India was studied using TMPA 3B42 V7 data sets from 1998 to 2013 and IMERG rainfall products from 2014 to 2017. It was observed that the satellite rainfall data sets provided adequate data sets with low bias and good agreement [73]. CHIRPS product was found to estimate on par with AWS data in the maximum range, while the other three products were underestimated (Figures 8–10). In coastal areas of subtropical climates, CHIRPS performed better, and the findings of this study are in good agreement with those of the TRMM product, which offered superior performance in detecting convective precipitation in tropical or subtropical regions during warm seasons [40]. When detecting no-precipitation or minimal precipitation events, the CHIRPS product outperformed, i.e., the product successfully identified more than 90% of these events [74]. The results indicate that IMERGH and TRMM precipitation products could be used during low rainfall conditions and CHIRPS in high rainfall conditions. Our findings are consistent with a research from northern Iraq, where zone I (Z-I) had more severe droughts than zones II (Z-II) and III (Z-III). In comparison, the TRMM fits the Z-I and Z-II drought assessments better, whereas the CHIRPS fits the Z-III drought analysis better [75,76]. Even at a 5 mm/d threshold, GPM worked best for numerical evaluation of precipitation and event detection [50].

The per cent agreement between precipitation from precipitation production and observed values from AWS showed that IMERGH registered the highest agreement per cent of 89.76, followed by 82.54 by TRMM. CHIRPS and PERSIANN followed in line with lower values of 81.95 and 81.12 per cent, respectively, in 2015. In 2016, TRMM edged past IMERGH with the agreement of 82.25 and 80.99 per cent. On the other hand, PERSIANN and CHIRPS recorded comparatively lesser agreement of 80.58 and 79.47 per cent, respectively. During 2017, all the satellite precipitation products registered comparatively higher agreement of more than 80 per cent regarding AWS observations, with CHIRPS recording the maximum agreement of 81.37 per cent, followed by IMERGH, PERSIANN, and TRMM agreement of 80.95, 80.93, and 80.68 per cent.
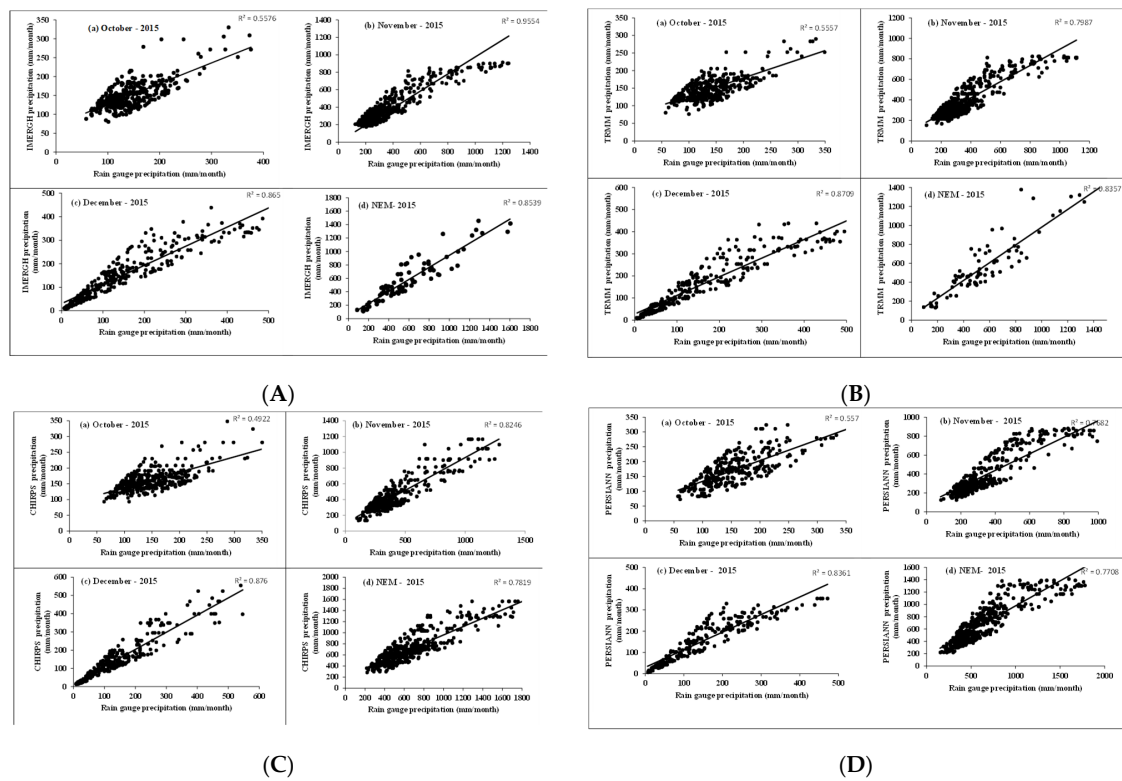
Figure 8. Scatter plots of monthly and accumulated rainfall for the year 2015 from rain-gauge stations vs. (**A**) IMERGH, (**B**) TRMM, (**C**) CHIRPS, (**D**)PERSIANN at the point-based station.
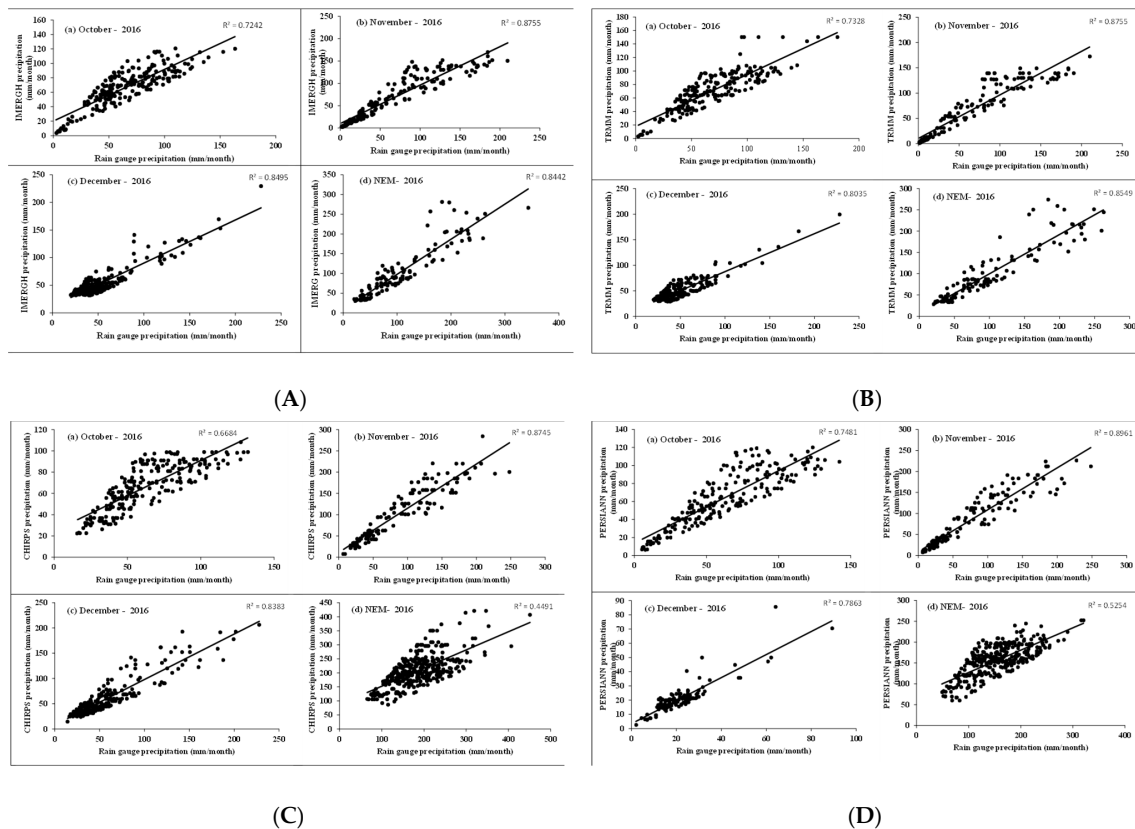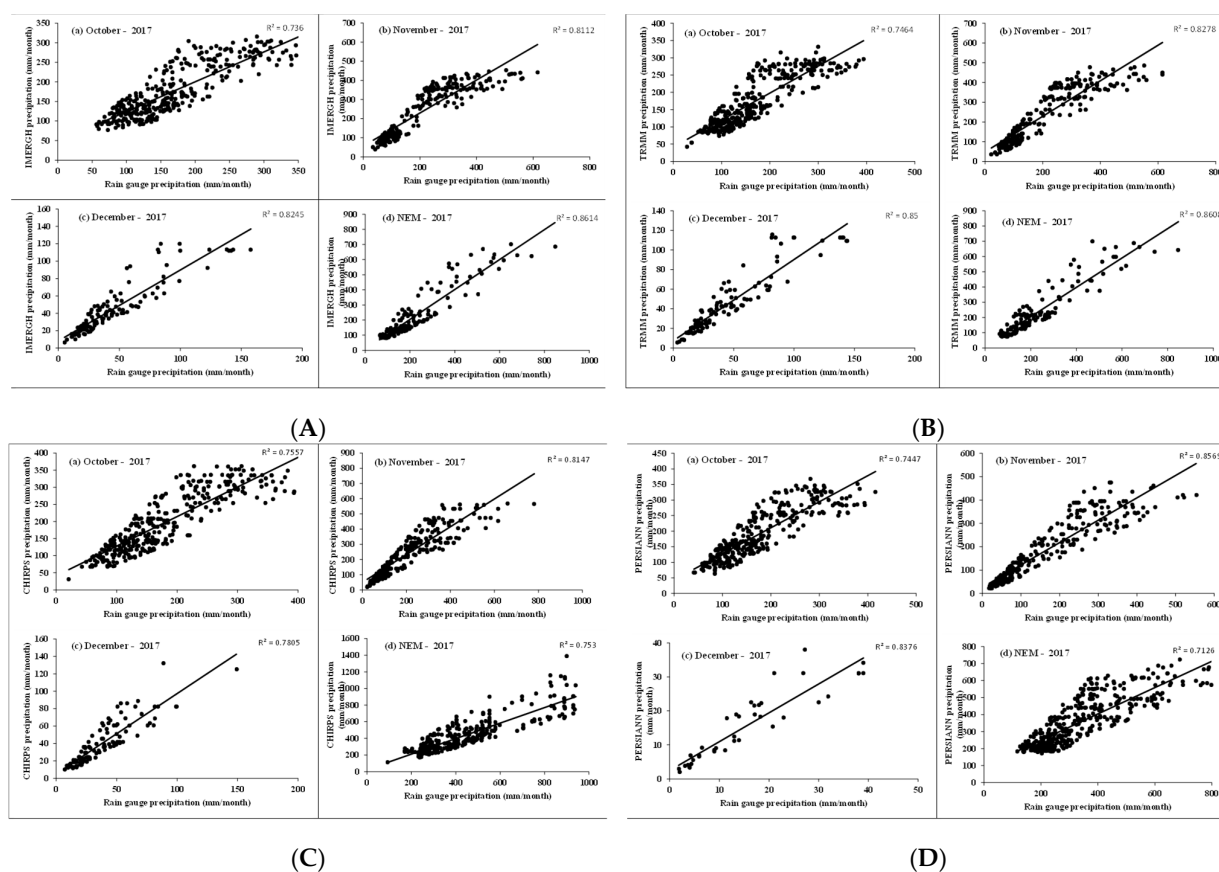

Figure 9. Scatter plots of monthly and accumulated rainfall for the year 2016 from rain-gauge stations vs. (**A**) IMERGH, (**B**) TRMM, (**C**) CHIRPS, (**D**) PERSIANN at the point-based station.

Figure 10. Scatter plots of monthly and accumulated rainfall for the year 2017 from rain-gauge stations vs. (**A**) IMERGH, (**B**) TRMM, (**C**) CHIRPS, (**D**) PERSIANN at the point-based station.

Among the HRPPs evaluated, CHIRPS data were found to have very good agreement with that of the AWS data, indicating the ability to accurately locate the spatial centres and accumulation of precipitation [77]. Such strong agreement between the identified drought and historical drought implies that CHIRPSv2 is a promising rainfall dataset that might be utilised to construct a drought monitoring and early warning system in Ethiopia [51,78]. The highest performance of CHIRPS over other products may be attributed to the development of the products derived from merging IR-derived precipitation with the climate hazards group precipitation climatology and blending with the ground station observation using the inverse distance weighted (IDW) method [27]. Irrespective of the study years, CHIRPS data agreement with AWS data was high compared to other precipitation products in all the agro-climatic zones of Tamil Nadu. In Cyprus, Katsanos et al. [65] carried out validation tests on CHIRPS products and reported good agreements with ground-based rain gauge data. Similarly, Pedreros et al. [79] found a higher correlation with ground-based data when validating CHIRPS over Colombia, particularly in drier months. Hessels [80] compared several open-source satellite products for the Nile basin and determined that CHIRPS was efficient for hydro-meteorological applications.

The general observation was that the SPI values were positive during the northeast monsoon of 2015 and varied between normal and extremely wet conditions, implying the possibility of normal vegetation growth during these months. On the other hand, the SPI values were negative for northeast monsoon of 2016 and 2017, representing mildly dry to extremely dry condition prevalence in the study region. According to Kumar et al. [56], the distinct intra-seasonal variability of 3-month SPI and IDMI was seen in 2016, which might be ascribed to the receipt of around 62.0% lower rainfall than the mean rainfall of Tamil Nadu's northeast monsoon season. The dry condition might indicate stressed vegetation due to a lack of water [71]. In an investigation, the SPI values plummeted from 0.03 to −0.15,

indicating an extremely dry condition triggered by insufficient precipitation [81]. From the results, it could be inferred that 2016 and 2017 were drought years during the northeast monsoon, and 2015 was non-drought. According to a study of rainfall anomalies during the Maha season in Sri Lanka, SPI values vary during drought and non-drought periods. The SPI value is low during the drought season, as seen in this case [82]. Since the 1-month time scale of SPI was used for assessing the drought years, the years identified as drought years could be designated agriculture drought years. SPI at block level resulted in 40, 120, and 127 blocks under extremely dry, severely dry, and moderately dry, respectively, during October 2016, and 91, 155, and 85 blocks under extremely dry, severely dry, and moderately dry, respectively, during November 2016, indicating severe drought conditions. SPI based on CHIRPSv2 accurately detected drought and non-drought years in river basins [51]. This variation benefited in determining the trend and the years when the area was more prone to drought owing to precipitation at block level.

From the results, it was concluded that the rainfall departure is the simplest method and was found to be efficient in identifying the meteorological drought in less time [83]. Pandit [84] evaluated the drought in the Maharashtra region of Solapur by comparing SPI and rainfall deviation. The study found a relationship between the positive values of rainfall deviation and the positive values of SPI, representing moisture or wetness for that specific year.

6. Conclusions

Drought can be observed effectively using drought indices, viz., Palmer drought severity index or the standardized precipitation index, calculated with in situ meteorological data from weather stations. The Palmer drought severity index utilizes the long-term historical rainfall data and mean temperature, which works based on a simple water balance model. In contrast, the standardized precipitation index adopts a temporally moving window method by aggregating the precipitation amount facilitating the outputs to be drawn at flexible time scales. In areas with sparse meteorological stations, drought conditions of unknown locations are estimated through spatial interpolation of known sampled data. However, the interpolation of meteorological data provides the details of the current drought condition, but it has high uncertainties since the interpolation is affected by many factors. Thus, remote sensing gained more attention for monitoring droughts, since it can be used to derive meteorological and biophysical information about terrestrial surfaces. In areas with limited meteorological stations, the remote sensing approach is the only source for drought monitoring. Using satellite-based rainfall estimates for drought monitoring has several advantages. Satellite derived rainfall products are useful for drought forecasting by overcoming the problem of unevenly distributed and erratic ground rain gauge measurements. These may provide an alternative for traditionally recorded rainfall at weather stations and enable global coverage to monitor large areas. Their daily coverage helps to monitor of the onset of drought events. On the other hand, they have few limitations; for example, rainfall estimates can have higher uncertainties, i.e., overestimation of low rainfall and under estimation of high rainfall values. These satellite-based rainfall products validation must be performed using in situ rain-gauge observations. The main findings from this study are:

- High-resolution precipitation products, IMERGH and TRMM, were on par with the minimum range predictions compared to AWS data. In contrast, the other two products (i.e.,) PERSIANN and CHIRPS overestimated the rainfall. On the other hand, the CHIRPS product was found to estimate on par with AWS data in the maximum range, while the other three products were underestimated. Therefore, IMERGH and TRMM precipitation products could be used during low rainfall conditions and CHIRPS in high rainfall conditions.
- The rainfall deviation during the northeast monsoon for the years 2016 and 2017 was mostly classified under deficient and large deficient categories showing moderate to severe drought conditions, with twelve, three, and fifteen districts under moderate

drought, and twenty, twenty-nine, and five districts under severe drought condition during October, November, and December 2016. During 2017, seventeen to twenty districts were under moderate drought conditions, and eight were under severe drought conditions.

- It is concluded that 2016 and 2017 were drought years in the northeast monsoon, and 2015 was a non-drought year in Tamil Nadu, India.

7. Future Scope

Further investigation is required on spatial patterns of rainfall using satellite products, in-depth research, or pixel-to-pixel analysis. It is possible to evaluate studies on establishing NDVI and NDWI using high resolution optical datasets to assess drought at the block or village level. The evaluation of the various satellite products during recent severe drought occurrences ought to be explored.

Author Contributions: Conceptualization, S.P. and V.G.; data curation, V.S., M.K. and R.K. (Ramalingam Kumaraperumal); formal analysis, V.S., S.P., V.G. and R.K. (Ramalingam Kumaraperumal); funding acquisition, S.P. and M.K.Y.; investigation, V.S. and S.P.; methodology, S.P., R.K. (Ramalingam Kumaraperumal), V.G. and V.S.; project administration, S.P., M.K.Y. and R.K. (Ragunath Kaliaperumal); resources, S.P. and V.S.; software, V.S., M.K., R.K. (Ramalingam Kumaraperumal) and R.K. (Ragunath Kaliaperumal); supervision, S.P., V.G., and R.K. (Ragunath Kaliaperumal); validation, S.P., V.S. and R.K. (Ramalingam Kumaraperumal); visualization, V.S. and R.K. (Ramalingam Kumaraperumal); writing—original draft, S.P., V.S. and R.K. (Ramalingam Kumaraperumal); writing—review and editing, S.P., V.S., M.K., M.R. and R.K. (Ramalingam Kumaraperumal). All authors have read and agreed to the published version of the manuscript.

Conflicts of Interest: The authors declare no conflict of interest.

References

1. Landrum, L.; Holland, M.M. Extremes become routine in an emerging new Arctic. *Nat. Clim. Change* **2020**, *10*, 1108–1115. [CrossRef]
2. Musolino, D.A.; Massarutto, A.; de Carli, A. Does drought always cause economic losses in agriculture? An empirical investigation on the distributive effects of drought events in some areas of Southern Europe. *Sci. Total Environ.* **2018**, *633*, 1560–1570. [CrossRef] [PubMed]
3. Wang, H.; Yang, X.; Chen, Q.; Su, J.-Q.; Mulla, S.I.; Rashid, A.; Hu, A.; Yu, C.-P. Response of prokaryotic communities to extreme precipitation events in an urban coastal lagoon: A case study of Yundang lagoon, China. *Sci. Total Environ.* **2020**, *706*, 135937. [CrossRef] [PubMed]
4. Zhong, R.; Chen, X.; Lai, C.; Wang, Z.; Lian, Y.; Yu, H.; Wu, X. Drought monitoring utility of satellite-based precipitation products across mainland China. *J. Hydrol.* **2019**, *568*, 343–359. [CrossRef]
5. Dahri, Z.H.; Ludwig, F.; Moors, E.; Ahmad, S.; Ahmad, B.; Ahmad, S.; Riaz, M.; Kabat, P. Climate change and hydrological regime of the high-altitude Indus basin under extreme climate scenarios. *Sci. Total Environ.* **2021**, *768*, 144467. [CrossRef]
6. Dai, A. Increasing drought under global warming in observations and models. *Nat. Clim. Change* **2013**, *3*, 52–58. [CrossRef]
7. Kulkarni, A.; Gadgil, S.; Patwardhan, S. Monsoon variability, the 2015 Marathwada drought and rainfed agriculture. *Curr. Sci.* **2016**, *111*, 1182–1193. [CrossRef]
8. Khosravi, H.; Haydari, E.; Shekoohizadegan, S.; Zareie, S. Assessment the effect of drought on vegetation in desert area using landsat data. *Egypt. J. Remote Sens. Space Sci.* **2017**, *20*, S3–S12. [CrossRef]
9. Jayasree, V.; Venkatesh, B. Analysis of rainfall in assessing the drought in semi-arid region of Karnataka State, India. *Water Resour. Manag.* **2015**, *29*, 5613–5630. [CrossRef]
10. Government of Tamil Nadu (GoT). Tamil Nadu Government Gazette. Published 18 January 2017. 2017. Available online: http://www.stationeryprinting.tn.gov.in/extraordinary/extraord_list2017.php (accessed on 17 December 2017).
11. Prakash, S.; Mitra, A.K.; Pai, D.; AghaKouchak, A. From TRMM to GPM: How well can heavy rainfall be detected from space? *Adv. Water Resour.* **2016**, *88*, 1–7. [CrossRef]

12. Sun, Q.; Miao, C.; Duan, Q.; Ashouri, H.; Sorooshian, S.; Hsu, K.L. A review of global precipitation data sets: Data sources, estimation, and intercomparisons. *Rev. Geophys.* **2018**, *56*, 79–107. [CrossRef]

13. Fang, J.; Yang, W.; Luan, Y.; Du, J.; Lin, A.; Zhao, L. Evaluation of the TRMM 3B42 and GPM IMERG products for extreme precipitation analysis over China. *Atmos. Res.* **2019**, *223*, 24–38. [CrossRef]

14. Shen, H.; Tabios, G., III. *Modeling of Precipitation-Based Drought Characteristics over California*; Centers for Water and Wildland Resources: Davis, CA, USA, 1996.

15. Tian, Y.; Xu, Y.-P.; Wang, G. Agricultural drought prediction using climate indices based on Support Vector Regression in Xiangjiang River basin. *Sci. Total Environ.* **2018**, *622*, 710–720. [CrossRef]

16. Sapiano, M.; Arkin, P. An intercomparison and validation of high-resolution satellite precipitation estimates with 3-hourly gauge data. *J. Hydrometeorol.* **2009**, *10*, 149–166. [CrossRef]

17. Tobin, K.J.; Bennett, M.E. Adjusting satellite precipitation data to facilitate hydrologic modeling. *J. Hydrometeorol.* **2010**, *11*, 966–978. [CrossRef]

18. Yin, J.; Guo, S.; Gu, L.; Zeng, Z.; Liu, D.; Chen, J.; Shen, Y.; Xu, C.-Y. Blending multi-satellite, atmospheric reanalysis and gauge precipitation products to facilitate hydrological modelling. *J. Hydrol.* **2021**, *593*, 125878. [CrossRef]

19. Yong, B.; Hong, Y.; Ren, L.L.; Gourley, J.J.; Huffman, G.J.; Chen, X.; Wang, W.; Khan, S.I. Assessment of evolving TRMM-based multisatellite real-time precipitation estimation methods and their impacts on hydrologic prediction in a high latitude basin. *J. Geophys. Res. Atmos.* **2012**, *117*, D9. [CrossRef]

20. Li, L.; Ngongondo, C.S.; Xu, C.-Y.; Gong, L. Comparison of the global TRMM and WFD precipitation datasets in driving a large-scale hydrological model in southern Africa. *Hydrol. Res.* **2013**, *44*, 770–788. [CrossRef]

21. Liang, Z.; Chen, S.; Yang, Y.; Zhao, R.; Shi, Z.; Rossel, R.A.V. National digital soil map of organic matter in topsoil and its associated uncertainty in 1980's China. *Geoderma* **2019**, *335*, 47–56. [CrossRef]

22. Zhou, Y.; Biswas, A.; Ma, Z.; Lu, Y.; Chen, Q.; Shi, Z. Revealing the scale-specific controls of soil organic matter at large scale in Northeast and North China Plain. *Geoderma* **2016**, *271*, 71–79. [CrossRef]

23. Belabid, N.; Zhao, F.; Brocca, L.; Huang, Y.; Tan, Y. Near-real-time flood forecasting based on satellite precipitation products. *Remote Sens.* **2019**, *11*, 252. [CrossRef]

24. Quintero, F.; Krajewski, W.F.; Mantilla, R.; Small, S.; Seo, B.-C. A spatial–dynamical framework for evaluation of satellite rainfall products for flood prediction. *J. Hydrometeorol.* **2016**, *17*, 2137–2154. [CrossRef]

25. Huffman, G.J.; Bolvin, D.T.; Braithwaite, D.; Hsu, K.; Joyce, R.; Xie, P.; Yoo, S.-H. *NASA Global Precipitation Measurement (GPM) Integrated Multi-Satellite Retrievals for GPM (IMERG)*; Algorithm Theoretical Basis Document (ATBD) Version 4; National Aeronautics and Space Administration: Washington, DC, USA, 2015.

26. Funk, C.C.; Peterson, P.J.; Landsfeld, M.F.; Pedreros, D.H.; Verdin, J.P.; Rowland, J.D.; Romero, B.E.; Husak, G.J.; Michaelsen, J.C.; Verdin, A.P. A quasi-global precipitation time series for drought monitoring. *US Geol. Surv. Data Ser.* **2014**, *832*, 1–12.

27. Funk, C.; Peterson, P.; Landsfeld, M.; Pedreros, D.; Verdin, J.; Shukla, S.; Husak, G.; Rowland, J.; Harrison, L.; Hoell, A. The climate hazards infrared precipitation with stations—A new environmental record for monitoring extremes. *Sci. Data* **2015**, *2*, 1–21. [CrossRef]

28. Huffman, G.J.; Bolvin, D.T.; Nelkin, E.J.; Wolff, D.B.; Adler, R.F.; Gu, G.; Hong, Y.; Bowman, K.P.; Stocker, E.F. The TRMM multisatellite precipitation analysis (TMPA): Quasi-global, multiyear, combined-sensor precipitation estimates at fine scales. *J. Hydrometeorol.* **2007**, *8*, 38–55. [CrossRef]

29. Joyce, R.J.; Janowiak, J.E.; Arkin, P.A.; Xie, P. CMORPH: A method that produces global precipitation estimates from passive microwave and infrared data at high spatial and temporal resolution. *J. Hydrometeorol.* **2004**, *5*, 487–503. [CrossRef]

30. Miller, S.; Arkin, P.; Joyce, R. A combined microwave/infrared rain rate algorithm. *Int. J. Remote Sens.* **2001**, *22*, 3285–3307. [CrossRef]

31. Hsu, K.-L.; Gao, X.; Sorooshian, S.; Gupta, H.V. Precipitation estimation from remotely sensed information using artificial neural networks. *J. Appl. Meteorol.* **1997**, *36*, 1176–1190. [CrossRef]

32. Sharifi, E.; Steinacker, R.; Saghafian, B. Assessment of GPM-IMERG and other precipitation products against gauge data under different topographic and climatic conditions in Iran: Preliminary results. *Remote Sens.* **2016**, *8*, 135. [CrossRef]

33. Brasil Neto, R.M.; Santos, C.A.G.; Silva, J.F.C.B.d.C.; da Silva, R.M.; Dos Santos, C.A.C.; Mishra, M. Evaluation of the TRMM product for monitoring drought over Paraíba State, northeastern Brazil: A trend analysis. *Sci. Rep.* **2021**, *11*, 1–18. [CrossRef]

34. Yu, C.; Hu, D.; Liu, M.; Wang, S.; Di, Y. Spatio-temporal accuracy evaluation of three high-resolution satellite precipitation products in China area. *Atmos. Res.* **2020**, *241*, 104952. [CrossRef]

35. Sharma, S.; Chen, Y.; Zhou, X.; Yang, K.; Li, X.; Niu, X.; Hu, X.; Khadka, N. Evaluation of GPM-Era satellite precipitation products on the southern slopes of the Central Himalayas against rain gauge data. *Remote Sens.* **2020**, *12*, 1836. [CrossRef]

36. Guo, R.; Liu, Y. Evaluation of satellite precipitation products with rain gauge data at different scales: Implications for hydrological applications. *Water* **2016**, *8*, 281. [CrossRef]

37. Gao, Y.; Liu, M. Evaluation of high-resolution satellite precipitation products using rain gauge observations over the Tibetan Plateau. *Hydrol. Earth Syst. Sci.* **2013**, *17*, 837–849. [CrossRef]

38. Liu, C.-Y.; Aryastana, P.; Liu, G.-R.; Huang, W.-R. Assessment of satellite precipitation product estimates over Bali Island. *Atmos. Res.* **2020**, *244*, 105032. [CrossRef]

39. Derin, Y.; Anagnostou, E.; Berne, A.; Borga, M.; Boudevillain, B.; Buytaert, W.; Chang, C.-H.; Delrieu, G.; Hong, Y.; Hsu, Y.C. Multiregional satellite precipitation products evaluation over complex terrain. *J. Hydrometeorol.* **2016**, *17*, 1817–1836. [CrossRef]

40. Bai, L.; Shi, C.; Li, L.; Yang, Y.; Wu, J. Accuracy of CHIRPS satellite-rainfall products over mainland China. *Remote Sens.* **2018**, *10*, 362. [CrossRef]

41. Zhu, Q.; Luo, Y.; Zhou, D.; Xu, Y.-P.; Wang, G.; Gao, H. Drought monitoring utility using satellite-based precipitation products over the Xiang River Basin in China. *Remote Sens.* **2019**, *11*, 1483. [CrossRef]

42. Prakash, S.; Gairola, R. Validation of TRMM-3B42 precipitation product over the tropical Indian Ocean using rain gauge data from the RAMA buoy array. *Theor. Appl. Climatol.* **2014**, *115*, 451–460. [CrossRef]

43. AghaKouchak, A. A baseline probabilistic drought forecasting framework using standardized soil moisture index: Application to the 2012 United States drought. *Hydrol. Earth Syst. Sci.* **2014**, *18*, 2485–2492. [CrossRef]

44. Vicente-Serrano, S.M.; Beguería, S.; López-Moreno, J.I. A multiscalar drought index sensitive to global warming: The standardized precipitation evapotranspiration index. *J. Clim.* **2010**, *23*, 1696–1718. [CrossRef]

45. Tadesse, T.; Brown, J.F.; Hayes, M.J. A new approach for predicting drought-related vegetation stress: Integrating satellite, climate, and biophysical data over the US central plains. *ISPRS J. Photogramm. Remote Sens.* **2005**, *59*, 244–253. [CrossRef]

46. McKee, T.B.; Doesken, N.J.; Kleist, J. The relationship of drought frequency and duration to time scales. In Proceedings of the 8th Conference on Applied Climatology, Anaheim, CA, USA, 17–22 January 1993; pp. 179–183.

47. Hayes, M.; Svoboda, M.; Wall, N.; Widhalm, M. The Lincoln declaration on drought indices: Universal meteorological drought index recommended. *Bull. Am. Meteorol. Soc.* **2011**, *92*, 485–488. [CrossRef]

48. Damberg, L.; AghaKouchak, A. Global trends and patterns of drought from space. *Theor. Appl. Climatol.* **2014**, *117*, 441–448. [CrossRef]

49. Alizadeh, M.R.; Nikoo, M.R. A fusion-based methodology for meteorological drought estimation using remote sensing data. *Remote Sens. Environ.* **2018**, *211*, 229–247. [CrossRef]

50. Chen, S.; Li, Q.; Zhong, W.; Wang, R.; Chen, D.; Pan, S. Improved monitoring and assessment of meteorological drought based on multi-source fused precipitation data. *Int. J. Environ. Res. Public Health* **2022**, *19*, 1542. [CrossRef]

51. Lemma, E.; Upadhyaya, S.; Ramsankaran, R. Meteorological drought monitoring across the main river basins of Ethiopia using satellite rainfall product. *Environ. Syst. Res.* **2022**, *11*, 1–15. [CrossRef]

52. Palagiri, H.; Pal, M. Agricultural Drought Monitoring using Satellite based Surface Soil Moisture Data. In Proceedings of the EGU General Assembly 2023, Vienna, Austria, 24–28 April 2023. EGU23-621. [CrossRef]

53. Galkate, R.; Jain, S.; Jaiswal, R.; Pandey, R.; Lohani, A.; Yadav, S.; Yadava, R.N. Application of GIS and Remote Sensing Tools in Assessment of Drought Using Satellite and Ground-Based Data. In *Application of Remote Sensing and GIS in Natural Resources and Built Infrastructure Management*; Springer: Berlin/Heidelberg, Germany, 2023; pp. 105–121.

54. Hakam, O.; Baali, A.; Azennoud, K.; Lyazidi, A.; Bourchachen, M. Assessments of Drought Effects on Plant Production Using Satellite Remote Sensing Technology, GIS and Observed Climate Data in Northwest Morocco, Case of the Lower Sebou Basin. *Int. J. Plant Prod.* **2023**, 1–16. [CrossRef]

55. Lakshmi, S.V.; Ramalakshmi, M.; Rakshith, R.K.; Christobel, M.J.; Kumar, P.P.; Priyadharshini, B.; Kumar, P.R. An integration of geospatial technology and standard precipitation index (SPI) for drought vulnerability assessment for a part of Namakkal district, South India. *Mater. Today: Proc.* **2020**, *33*, 1206–1211.

56. Kumar, K.A.; Reddy, G.O.; Masilamani, P.; Turkar, S.Y.; Sandeep, P. Integrated drought monitoring index: A tool to monitor agricultural drought by using time-series datasets of space-based earth observation satellites. *Adv. Space Res.* **2021**, *67*, 298–315. [CrossRef]

57. Kumaraperumal, R.; Pazhanivelan, S.; Ragunath, K.P.; Kannan, B.; Prajesh, P.J.; Mugilan, G.R. Agricultural drought monitoring in Tamil Nadu in India using Satellite-based multi vegetation indices. *J. Appl. Nat. Sci.* **2021**, *13*, 414–423. [CrossRef]

58. Thilagaraj, P.; Masilamani, P.; Venkatesh, R.; Killivalavan, J. Google Earth Engine Based Agricultural Drought Monitoring in Kodavanar Watershed, Part of Amaravathi Basin, Tamil Nadu, India. *Int. Arch. Photogramm. Remote Sens. Spat. Inf. Sci.* **2021**, *43*, 43–49. [CrossRef]

59. Hou, A.Y.; Kakar, R.K.; Neeck, S.; Azarbarzin, A.A.; Kummerow, C.D.; Kojima, M.; Oki, R.; Nakamura, K.; Iguchi, T. The global precipitation measurement mission. *Bull. Am. Meteorol. Soc.* **2014**, *95*, 701–722. [CrossRef]

60. Huffman, G.J.; Adler, R.F.; Bolvin, D.T.; Nelkin, E.J. The TRMM multi-satellite precipitation analysis (TMPA). In *Satellite Rainfall Applications for Surface Hydrology*; Springer: Berlin/Heidelberg, Germany, 2010; pp. 3–22.

61. Huffman, G.J.; Adler, R.F.; Rudolf, B.; Schneider, U.; Keehn, P.R. Global precipitation estimates based on a technique for combining satellite-based estimates, rain gauge analysis, and NWP model precipitation information. *J. Clim.* **1995**, *8*, 1284–1295. [CrossRef]

62. Huffman, G.J.; Adler, R.F.; Arkin, P.; Chang, A.; Ferraro, R.; Gruber, A.; Janowiak, J.; McNab, A.; Rudolf, B.; Schneider, U. The global precipitation climatology project (GPCP) combined precipitation dataset. *Bull. Am. Meteorol. Soc.* **1997**, *78*, 5–20. [CrossRef]

63. Seiler, R.; Hayes, M.; Bressan, L. Using the standardized precipitation index for flood risk monitoring. *Int. J. Climatol. A J. R. Meteorol. Soc.* **2002**, *22*, 1365–1376. [CrossRef]

64. Lovett, G.; Burns, D.; Driscoll, C.; Jenkins, J.; Mitchell, M.; Rustad, L.; Shanley, J.; Likens, G.; Haeuber, R. Who needs environmental monitoring? *Front. Ecol. Environ.* **2007**, *5*, 253–260. [CrossRef]

65. Katsanos, D.; Retalis, A.; Michaelides, S. Validation of a high-resolution precipitation database (CHIRPS) over Cyprus for a 30-year period. *Atmos. Res.* **2016**, *169*, 459–464. [CrossRef]

66. Sorooshian, S.; Hsu, K.-L.; Gao, X.; Gupta, H.V.; Imam, B.; Braithwaite, D. Evaluation of PERSIANN system satellite-based estimates of tropical rainfall. *Bull. Am. Meteorol. Soc.* **2000**, *81*, 2035–2046. [CrossRef]
67. Yang, T.; Zhang, W.; Zhou, T.; Wu, W.; Liu, T.; Sun, C. Plant phenomics & precision agriculture simulation of winter wheat growth by the assimilation of unmanned aerial vehicle imagery into the WOFOST model. *PLoS ONE* **2021**, *16*, e0246874.
68. Araujo, J.; Born, D.G. Calculating percentage agreement correctly but writing its formula incorrectly. *Behav. Anal.* **1985**, *8*, 207. [CrossRef] [PubMed]
69. IMD. *Climate Diagnostic Bulletin of India, India Meteorological Department. June, July, August 1971*; Rep. No. 88, 89 and 90; Nat. Climate Centre, IMD: Pune, India, 1971.
70. Bordi, I.; Frigio, S.; Parenti, P.; Speranza, A.; Sutera, A. The analysis of the Standardized Precipitation Index in the Mediterranean area: Large-scale patterns. *Ann. Geophys.* **2001**, *44*. [CrossRef]
71. Karinki, R.K.; Sahoo, S.N. Use of meteorological data for identification of drought. *ISH J. Hydraul. Eng.* **2021**, *27*, 427–433. [CrossRef]
72. Prakash, S.; Mitra, A.K.; AghaKouchak, A.; Liu, Z.; Norouzi, H.; Pai, D. A preliminary assessment of GPM-based multi-satellite precipitation estimates over a monsoon dominated region. *J. Hydrol.* **2018**, *556*, 865–876. [CrossRef]
73. Kumar, T.V.L.; Barbosa, H.A.; Thakur, M.K.; Paredes-Trejo, F. Validation of satellite (TMPA and IMERG) rainfall products with the IMD gridded data sets over monsoon core region of India. In *Satellite Information Classification and Interpretation*; IntechOpen: London, UK, 2019.
74. Ghozat, A.; Sharafati, A.; Hosseini, S.A. Long-term spatiotemporal evaluation of CHIRPS satellite precipitation product over different climatic regions of Iran. *Theor. Appl. Climatol.* **2021**, *143*, 211–225. [CrossRef]
75. Suliman, A.H.A.; Awchi, T.A.; Al-Mola, M.; Shahid, S. Evaluation of remotely sensed precipitation sources for drought assessment in Semi-Arid Iraq. *Atmos. Res.* **2020**, *242*, 105007. [CrossRef]
76. Awchi, T.; Suliman, A. Spatiotemporal assessment of meteorological drought using satellite-based precipitation data over Iraq. In Proceedings of the IOP Conference Series: Earth and Environmental Science, Surakarta, Indonesia, 24–25 August 2021; p. 012052.
77. Gao, F.; Zhang, Y.; Ren, X.; Yao, Y.; Hao, Z.; Cai, W. Evaluation of CHIRPS and its application for drought monitoring over the Haihe River Basin, China. *Nat. Hazards* **2018**, *92*, 155–172. [CrossRef]
78. Shalishe, A.; Bhowmick, A.; Elias, K. Meteorological Drought Monitoring Based on Satellite CHIRPS Product over Gamo Zone, Southern Ethiopia. *Adv. Meteorol.* **2022**, *2022*, 9323263. [CrossRef]
79. Pedreros, D.H.; Rojas, A.; Funk, C.; Peterson, P.; Landsfeld, M.F.; Husak, G.J. The Use of CHIRPS to Analyze Historical Rainfall in Colombia. In Proceedings of the AGU Fall Meeting Abstracts, San Francisco, CA, USA, 15–19 December 2014; GC33C-0534. American Geophysical Union: San Francisco, CA, USA, 2014.
80. Hessels, T.M. Comparison and Validation of Several Open Access Remotely Sensed Rainfall Products for the Nile Basin. Master's Thesis, TU Delft Library, Delft, The Netherlands, 2015.
81. Ainembabazi, S. Comparison of Standardized Precipitation Index (SPI) and Vegetation Health Index (VHI) in Drought Monitoring in Isingiro District. Ph.D. Thesis, Makerere University, Kampala, Uganda, 2022.
82. Alahacoon, N.; Edirisinghe, M.; Ranagalage, M. Satellite-based meteorological and agricultural drought monitoring for agricultural sustainability in Sri Lanka. *Sustainability* **2021**, *13*, 3427. [CrossRef]
83. Zargar, A.; Sadiq, R.; Naser, B.; Khan, F.I. A review of drought indices. *Environ. Rev.* **2011**, *19*, 333–349. [CrossRef]
84. Pandit, D.V. Assessment of Meteorological Drought for Semi-Arid Region of Maharashtra. *Int. J. Agric. Environ. Biotechnol.* **2018**, *11*, 689–695. [CrossRef]